AD-A065 303 ROCKWELL INTERNATIONAL ANAHEIM CA ELECTRONICS RESEAR--ETC F/G 17/2
BISMUTH GERMANIUM OXIDE (BGO) SURFACE ACOUSTIC WAVE (SAW) CONVO--ETC(U)
FEB 79 L R ADKINS DASG60-77-C-0115
UNCLASSIFIED C79-118/501 NL

| OF |
AD
AD65303

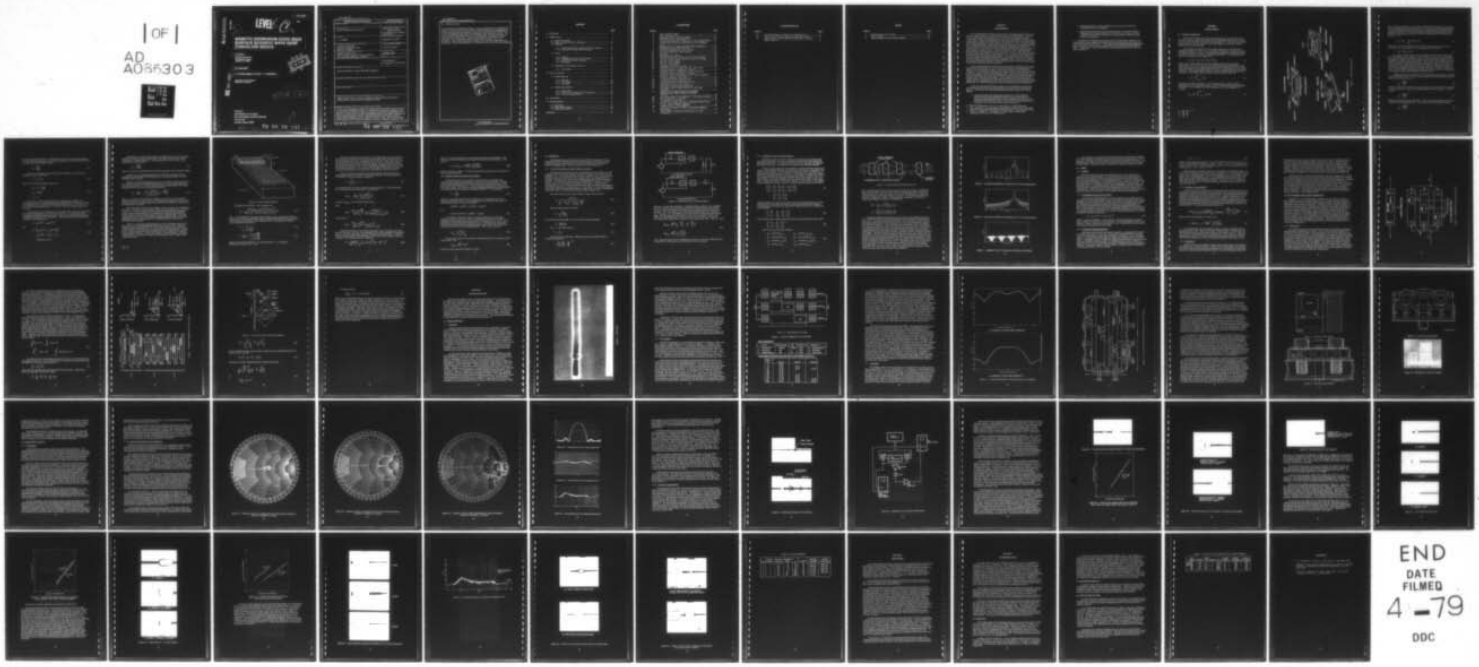

END
DATE FILMED
4-79
DDC

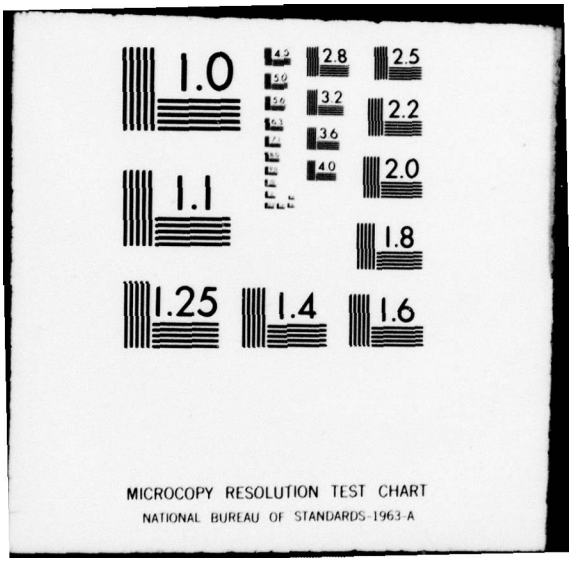
1.0
2.8
2.5
3.2
2.2
3.6
2.0
4.0
1.1
1.8
1.25
1.4
1.6
MICROCOPY RESOLUTION TEST CHART
NATIONAL BUREAU OF STANDARDS-1963-A

LEVEL II

BISMUTH GERMANIUM OXIDE (BGO) SURFACE ACOUSTIC WAVE (SAW) CONVOLVER DEVICE

10 L. R. Adkins
Rockwell International
3370 Miraloma Avenue
Anaheim, CA 92803

11 16 February 1979

9 Final Report for Period 15 July 1977 – 31 October 1978

Approved for Public Release
Distribution Unlimited

12 67 P.

15 DASG60-77-C-0115

16 [illegible]

Prepared for
DEPARTMENT OF THE ARMY
BALLISTIC MISSILE SYSTEM COMMAND
P/O Box 1500
Huntsville, Alabama, 35807

UNCLASSIFIED

SECURITY CLASSIFICATION OF THIS PAGE *(When Data Entered)*

REPORT DOCUMENTATION PAGE		READ INSTRUCTIONS BEFORE COMPLETING FORM
1. REPORT NUMBER	2. GOVT ACCESSION NO.	3. RECIPIENT'S CATALOG NUMBER
4. TITLE *(and Subtitle)* BGO/SAW CONVOLVER DEVICE		5. TYPE OF REPORT & PERIOD COVERED Final July 15, 1977- October 31, 1978
		6. PERFORMING ORG. REPORT NUMBER C79-118/501
7. AUTHOR(s) L. R. Adkins		8. CONTRACT OR GRANT NUMBER(s) DASG60-77-C-0115
9. PERFORMING ORGANIZATION NAME AND ADDRESS Rockwell International Electronics Research Center Anaheim, CA 92803		10. PROGRAM ELEMENT, PROJECT, TASK AREA & WORK UNIT NUMBERS Project No. 79571
11. CONTROLLING OFFICE NAME AND ADDRESS Department of the Army Ballistic Missile Defense Systems Command P.O. Box 1500, Huntsville, Ala 35807		12. REPORT DATE December 1978 13. NUMBER OF PAGES 60
14. MONITORING AGENCY NAME & ADDRESS*(if different from Controlling Office)*		15. SECURITY CLASS. *(of this report)* UNCLASSIFIED 15a. DECLASSIFICATION/DOWNGRADING SCHEDULE

16. DISTRIBUTION STATEMENT *(of this Report)*

Approved for public release, distribution unlimited

17. DISTRIBUTION STATEMENT *(of the abstract entered in Block 20, if different from Report)*

18. SUPPLEMENTARY NOTES

19. KEY WORDS *(Continue on reverse side if necessary and identify by block number)*

Surface acoustic wave, convolver, nonlinear surface acoustic wave devices, matched filters, piezoelectric-semiconductor devices

20. ABSTRACT *(Continue on reverse side if necessary and identify by block number)*

This report describes the design and evaluation of strip-coupled convolvers (SCCs) with large time-bandwidth products. A multichannel concept was developed for this project in order to reduce the deleterious effects and fabrication complexities due to extensive metallization in the acoustic propagation paths (an inevitable consequence of SCCs with long interaction times). With this approach the interaction region is divided among N separate convolver channels, each covering 1/Nth of the total interaction region, and the respective outputs are summed. Using this technique, SCCs

DD FORM 1 JAN 73 1473 EDITION OF 1 NOV 65 IS OBSOLETE

UNCLASSIFIED

SECURITY CLASSIFICATION OF THIS PAGE *(When Data Entered)*

20. ABSTRACT (Cont)

with equivalent time-bandwidth products in excess of 1000 have been demonstrated. Further, with the best device, the nonlinear coupling coefficient M was found to be of the theoretical order of magnitude, and to have internal conversion efficiencies an order of magnitude better than corresponding air-gap convolvers (AGCs). The results of these investigations led to the conclusion that, with optimum efficiency in the input and output circuits, large time-bandwidth (2000-5000) SCCs, with efficiencies up to 20 dB greater than currently available modes, are a real possibility. These higher efficiencies, together with relatively simple fabrication procedures, make the multichannel SCC an attractive device for further development.

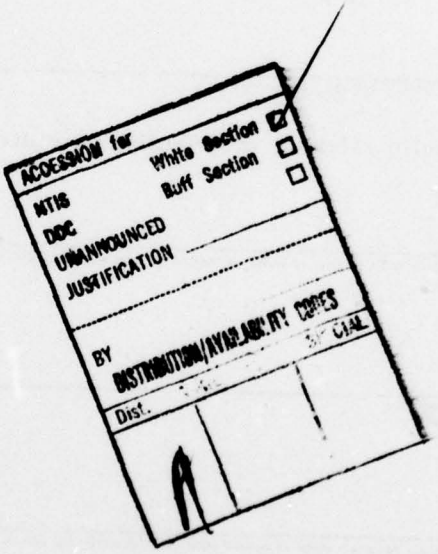

CONTENTS

ILLUSTRATIONS

ILLUSTRATIONS (Cont)

TABLES

SECTION I

INTRODUCTION

The acoustoelectric convolver has been found to be highly effective for processing long, coded waveforms in spread-spectrum communication systems. The convolver approach now being evaluated in such systems is a combination surface acoustic wave (SAW)/semiconductor device where the semiconductor is spaced above a piezoelectric surface and acoustoelectric interactions take place across the air gap. An alternate approach is the strip-coupled convolver (SCC). Here, the mode of operation is exactly analogous to that of the air-gap convolver (AGC), but differs from this device in that the electric field associated with the propagating acoustic wave is transferred over to a region of the device adjacent to the acoustic path by means of a large number of metallic strips. A number of authors[1-3] have investigated this device and have found that the efficiency of the SCC can be as much as two orders of magnitude greater than that of a corresponding AGC. However, most of these devices have had small time-bandwidth (TB) products. This has been the case because the maximum length of the signal capable of being processed by the device is determined by the time delay provided by the acoustic propagation path. For the SCC, a large time delay necessitates defining an extremely large number of narrow metallic strips on the surface of the piezoelectric substrate.

This report describes the result of a new approach for utilizing the SCC which enables one to obtain large TB, and still retain most of the increased efficiency. In essence, the total interaction region is split into N sections by utilizing N SCC's. These SCC's are all identical except that the coupling strips on each substrate occupy a different, unique location on the propagation path. As each set of strips cover 1/N of the required delay, the sum of the N outputs is equivalent to the output of a single convolver with a long interaction region. The advantage of this system is that a smaller number of strips must be fabricated for each section, thus making the fabrication problems manageable as well as reducing the deleterious effects such as losses, reflections, etc. which inevitably arise from an extended region of metallization.

In the work performed during this program, this multichannel approach has been demonstrated utilizing bismuth germanium oxide (BGO) as the piezoelectric material. We feel that the major accomplishments of this program have been as follows:

1. Demonstrating that the multichannel technique is a valid method for achieving large time-bandwidth products with strip-coupled devices. (Using this multichannel technique, we have evaluated SCC's having time bandwidth (TB) of from 83 to 1039. To the best of our knowledge these are the largest TB's ever reported for devices of this type.)

1. Kino, G. S. and Shreve, W. R., J. Appl. Phys. 44, 3960-3968 (1973).
2. Otto, Oberdan W., paper presented at Polytechnic Institute of New York, MRI Symposium on Optical and Acoustical Microelectronics, New York (April 1974).
3. Aoki, T., Matuda, M., and Hattari, S., IEEE Trans. on Sonics and Ultrasonics, SU-25, No. 4, 213-220 (1978).

2. Obtaining nonlinear coupling coefficients on the best device which has the theoretical order of magnitude.

3. Showing how the first two results imply that large-TB convolvers having bilinear conversion efficiencies from -60 dBm to -55 dBm (some 10 dB to 15 dB better than current modes) are a real possibility, provided external losses can be reduced.

In Section II, the design theory for these devices is presented. Section 2.1 of Section II describes the physical principals involved, while the multichannel approach is discussed in detail in Section 2.5. The results of the experimental investigations are given in Section III, with a concise summary of convolver results being presented in Table 1 in that section. Final conclusions and recommendations for future work are given in Section IV.

SECTION II

DESIGN THEORY

2.1 PHYSICAL PRINCIPLES

The physical mechanisms involved in producing the convolution/correlation function of two input signals with SAW devices (or with SAW/semiconductor combinations) have been described in detail by several authors[1-3]. Therefore, only a brief outline of acousto-electric convolver theory with emphasis on the strip-coupled approach will be presented here.

The simplest SAW convolver utilizes only a piezoelectric substrate and is configured as shown in Figure 1(a). Two signals of frequency ω are fed into the two interdigital transducers (IDT's), producing a pair of oppositely propagating surface acoustic strain waves, S_1 and S_2. The displacement field, D, in the region where the two waves interact can be shown to be

$$D = e(S_1 + S_2) + \epsilon(E_1 + E_2) + KS_1 S_2 \tag{1}$$

where e and ϵ are the piezoelectric strain constant and dielectric constant, respectively, and E_1 and E_2 are the two piezoelectrically generated electric fields. The final term in Eq. (1) is nonlinear and varies with a frequency of 2ω; K is a constant proportional to the strength of this term and is a strong function of the material employed. If a thin metal plate of length L is placed midway between the two input transducers, the voltage induced across this plate to ground is given by

$$V = \frac{w}{c} \int_{-L/2}^{L/2} D \, dZ \tag{2}$$

where w is the width of the plate, c is the total capacitance, and the Z axis is perpendicular to the crystalline surface. It can be shown that all terms oscillating at frequency ω are traveling waves and integrate to zero, so that equation (2) becomes

$$V_{2\omega} = \frac{w}{c} \int_{-L/2}^{L/2} D_{2\omega} \, dZ \tag{3}$$

---

1. Op. cit.
2. Op. cit.
3. Op. cit.

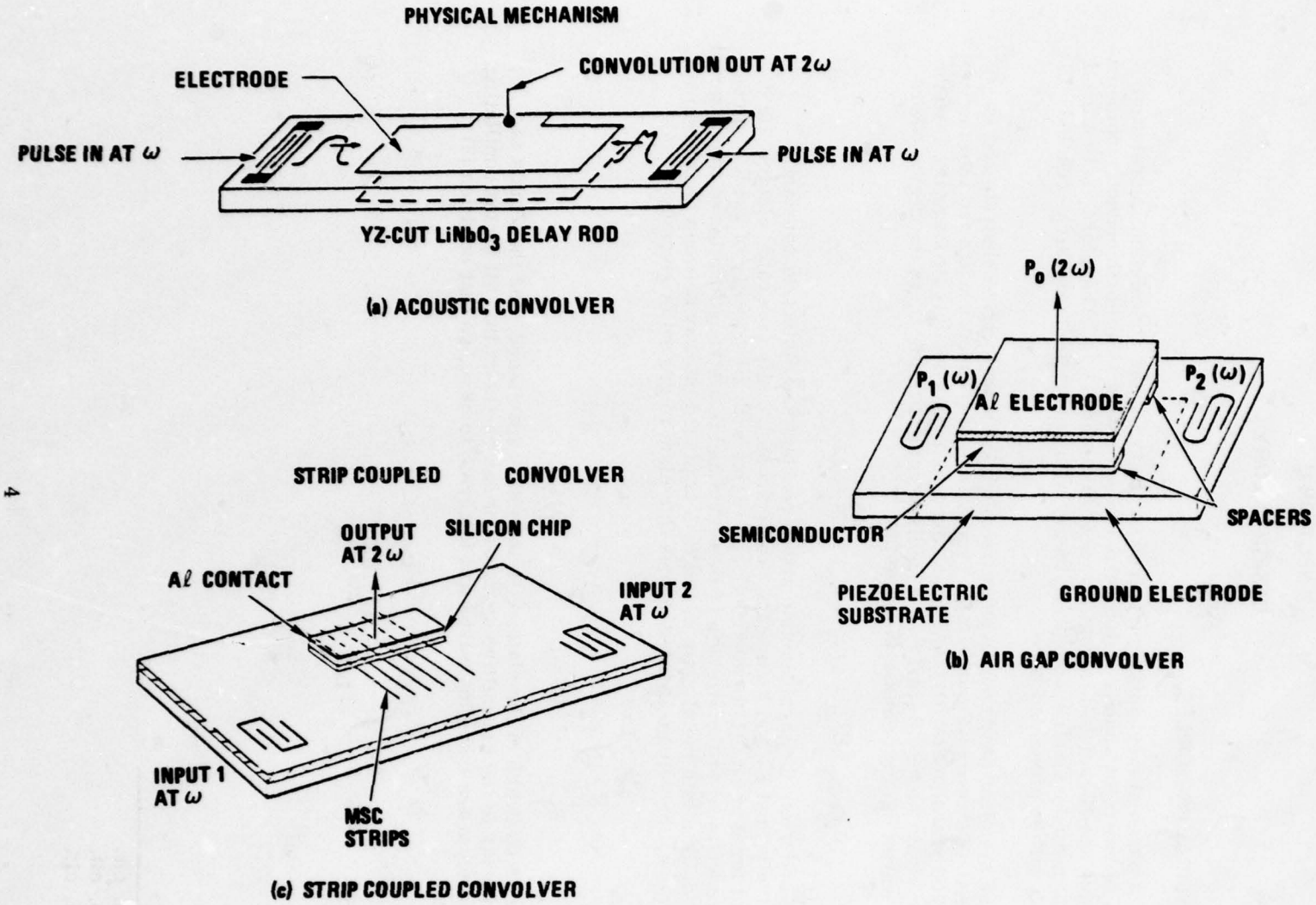

Figure 1. Three Convolver Types

Thus, the output voltage at 2ω is directly proportional to the integral of the product of the two oppositely-directed strain waves. The processes of shifting (represented by the two oppositely-directed traveling waves), multiplication (represented by the nonlinear interaction), and integration (represented by the voltage induced across the plate) are exactly those processes involved in obtaining the convolution of two functions. Thus,

$$V_2 \alpha\ h(t) = \int_{-\infty}^{\infty} f(t)\ g\ (t-\tau)d\tau \tag{4}$$

where h(t) is the usual symbol for the convolution of two functions f(t) and g(t). Correlation may be obtained by time reversing one of the functions

$$h(t) = \int f(t)\ g(\tau-t)d\tau \tag{5}$$

The simple acoustic convolver is not suitable for most systems applications, since the magnitude of the nonlinear interaction is very small. Thus, means have been sought to enhance the nonlinear effect, and these means have usually involved methods for coupling of the strain produced electric field to the strong space charge nonlinearities of semiconductor materials. The air-gap convolver (AGC) shown in Figure 1(b) utilizes a semiconductor (usually silicon) chip spaced a few tenths of microns above the surface of the piezoelectric substrate. The electric fields produced by the propagating strain waves interact with the semiconductor charge carriers, and the resultant voltage induced across the silicon to ground is proportional to the product of the normal components of the two fields.

Consider the normal component E_n of an electric field produced by a propagating surface acoustic wave. E_n will produce a depletion layer of thickness ℓ_D at the surface of the silicon given by

$$E_n = \frac{N_d q \ell_D}{\epsilon} \tag{6}$$

where N_d is the donor density for an n-type material, q is the electronic change and ϵ is the permittivity. If V_ℓ is the voltage developed across the layer, $E = V_\ell / \ell_D$ so that

$$V_\ell = \frac{N_d q \ell_D^{\,2}}{2\epsilon} \tag{7}$$

When the potential V_ℓ is very small ($V_\ell << kT/q$), the depletion layer will be much smaller than the Debyelength ($\ell_D << \lambda_d$), and Eq (7) must be modified to obtain

$$V_\ell = \frac{N_d q \ell_D^{\,2}}{6\epsilon}. \tag{8}$$

For the cases discussed here, V_ℓ will always be small, so Eq (8) will be taken as the basic defining relationship. To express the potential in terms of the field Eq (6) is substituted in Eq (8) and one obtains

$$V_\ell = \frac{\varepsilon E_n^2}{6qN_d} \tag{9}$$

It should be noted that the degrading effects of diffusion are assumed to be negligible, which will be true if

$$\omega << (\omega_D, \omega_M) \tag{10}$$

where ω is the operating radian frequency and

$$\begin{aligned} \omega_D &= v^2/D = \frac{v^2 q}{kT\mu} \\ \omega_M &= \sqrt{\omega_c \omega_D} \\ \omega_c &= \varepsilon/\sigma \end{aligned} \tag{11}$$

In Eq (11), v is the acoustic velocity, q is the electronic charge, k is Boltzman's constant, μ is the mobility of the semiconductor, σ its conductivity and ϵ its permittivity. For the materials discussed in this report $\omega_D \sim 10^{11}$, $\omega_M \sim 6 \times 10^{10}$, and the operating frequency $\omega \sim 2.5 \times 10^9$. Thus, any diffusion effects will be minor.

Returning to Eq (9), the field E_n at the silicon surface arises from the acoustic strain wave propagating on the piezoelectric substrate. Two such strain waves propagating in opposite directions along the x axis will have associated fields given by $E_1 e^{j(\omega t - kx)}$ and $E_2 e^{j(t+kx)}$, respectively. Thus, the total electric field from the crystal at a given point will be

$$E = E_1 e^{j(\omega t - kx)} + E_2 e^{j(\omega t + kx)} \tag{12}$$

and

$$\begin{aligned} E^2 &= \left[E_1 e^{j(\omega t - kx)} + E_2 e^{j(\omega t + kx)} \right]^2 \\ &= E_1 E_2 e^{j2\omega t} + 1/2(E_1^2 + E_2^2) \\ &\quad + \text{additional terms in x} \end{aligned} \tag{13}$$

Substituting Eq (13) into Eq (9) it will be seen that there is a term in the depletion layer potential expression proportional to the product of the two input waves oscillating at a radian frequency 2ω. For low signal levels the d-c term $\propto (E_1^2 + E_2^2)$ will not be important and

$$V_{2\omega} = \frac{E_1 E_2}{6qNd} \tag{14}$$

where E_1 and E_2 are understood to be the normal components of the respective fields.

Equation (14) is a general expression which holds for all transverse field piezoelectric-semiconductor convolution devices, assuming low signal levels and negligible diffusion effects.

However, to design an operating device it is necessary to be able to determine V_2 in terms of material parameter and input powers. It can be shown[1] that for an AGC with input powers P_1, P_2 watts and acoustic beam width b meters the voltage developed across the silicon chip to ground is given by

$$V_{2\omega} = \frac{8}{3qNd} \cdot \frac{(\varepsilon_o + \varepsilon_p)(\Delta V/V)\omega}{(1 + \varepsilon_p \beta h/\varepsilon_o)^2 \varepsilon_s v^2} \cdot \sqrt{\frac{P_1 P_2}{b}} \tag{15}$$

Here, ε_o, ε_p and ε_s are the dielectric constants of free space, the piezoelectric and the semiconductor, respectively; β is the propagation constant; v is the acoustic velocity; and h is the distance between the surface of the piezoelectric substrate and the facing surface of Si chip.

The strip-coupled convolver (SCC) shown in Figure 1(c) and 2 is a modification of the AGC. The basic mode of operation of the SCC is exactly the same as that of the AGC, but it differs in that the electric fields associated with the propagating surface waves are transferred over to a region of the substrate adjacent to the acoustic path by means of a large number of metallic coupling strips. Otto[2] has calculated the output of an SCC assuming an infinite number of strips per acoustic wavelengths; this is a useful approach for establishing ultimate limits on the efficiency of these devices.

However, for any practical application the number of coupling strips will be finite; the current photolithographic fabrication limit is about 2 μm. Thus, the original theoretical analysis of the SCC with a finite number of strips performed by Kino and Shreve[1] and Aoki et al[3] is appropriate for the present work. Recently, Aoki et al[3] have published a finite strip theory for the SCC based on a parametric circuit analysis approach. In these latter analyses, the determination of the field coupled onto the semiconductor surface requires summation over a large number of space harmonics.

---

[1] Op. cit.

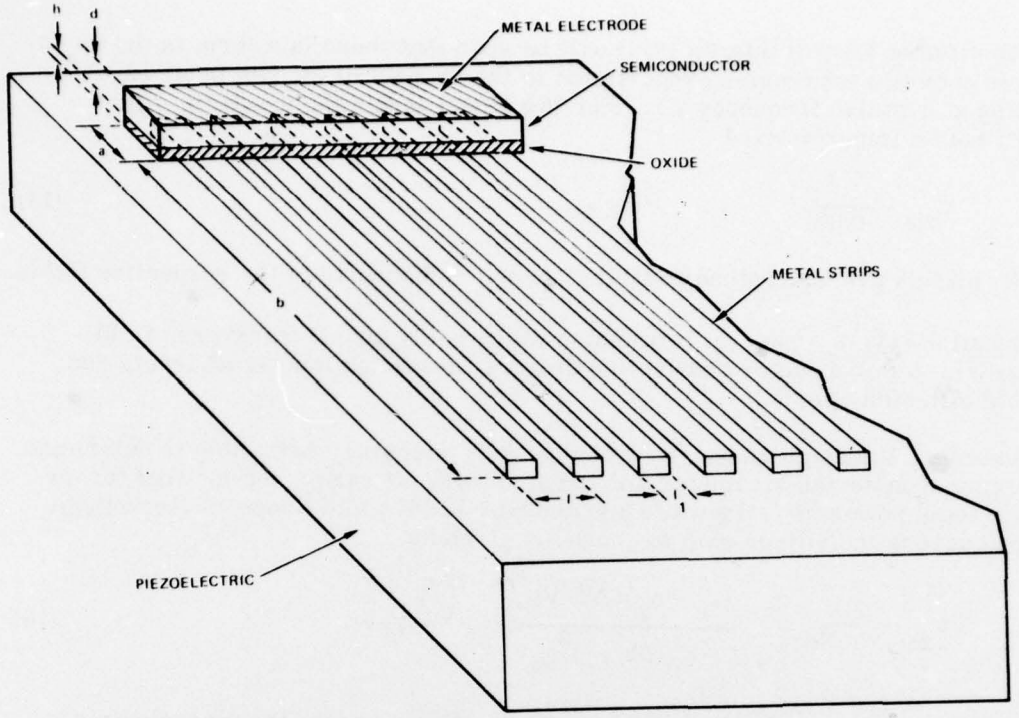

Figure 2. Strip-Coupled Convolver

Following Kino and Shreve, it can be shown that

$$V_{2\omega} = \frac{8\,(\Delta v/v)(\varepsilon_o + \varepsilon_p)\omega\, R^2\, \ell^2\, (P_1 P_2)^{1/2}}{3qNd\, \varepsilon_s\, v_s^2\quad M\ell\, a/b + \beta h\, \ell(\varepsilon_o + \varepsilon_p)/\varepsilon^{1\,2}} \tag{16}$$

Here, ε^1 is the dielectric constant of the oxide layer on the semiconductor surface, while R and M are parameters which contain Legendre polynominals whose arguments are functions of the geometry of the coupling structure and propagation constant. These parameters are given by

$$R = \frac{1}{P_{-\nu}\,(\cos\frac{\pi \ell 1}{\ell})} \tag{17}$$

$$M = \frac{\nu\pi}{\mathrm{Sin}\ \nu\pi}\quad \frac{P_{-\nu}(-\cos\frac{\pi\ell 1}{\ell})}{P_{-\nu}\,(\cos\frac{\pi\ell 1}{\rho})} \tag{18}$$

where ℓ is the strip periodicity, ℓ_1 is the strip width, $P_{-\nu}$ is a Legendre polynominal of order ν and $\nu = \ell/\lambda$.

There are two key factors in Eq (16). If h, the thickness of the oxide layer on the semiconductor surface is very small (less than 500Å), then the second term in the denominator brackets can be neglected and the value of V_2 for a given strip geometry and input power will be controlled by a/b, the ratio of width of the silicon under the coupling strips to the acoustic beamwidth. Comparing with Eq (15) it will be seen that the output of the SCC could be substantially greater than that of the AGC, other factors being equal. The reason for this increase in efficiency is a better impedance match between the acoustic and semiconductor region of the device.

In order to obtain an efficiency factor which depends only on material and geometrical parameters independent of input power levels, the expression for V_2 is divided by $[P_1 P_2/b]$ to obtain a constant M:

$$M = \frac{V_2}{(P_1 P_2)^{1/2}} \cdot b \tag{19}$$

M is usually referred to as the nonlinear coupling coefficient. In the MKS system it has dimensions of volt-meter/watt. From Eq (15),

$$M_{(AGC)} = \frac{8}{3qNd} \frac{(\varepsilon_o + \varepsilon_p)(\frac{\Delta v}{v})\,\omega}{(1+\varepsilon_p \beta h/\varepsilon_o)^2 \varepsilon_s v^2} \tag{20}$$

Similarly, $M_{(SCC)}$ can be obtained from Eq (16).

Thus,

$$M_{SCC} = \frac{\omega(\varepsilon_o + \varepsilon_p)\,(\frac{\Delta v}{v})}{3qNd\ \varepsilon_s\ v_s^2} \frac{R^2(\ell/\ell_1)^2}{[M\,a/b + \beta h(\ell/\ell_1)(\varepsilon_o + \varepsilon_p)\varepsilon_o^{-1}]^2} \tag{21a}$$

in the limit $h \ll 1$

$$M_{SCC} = \frac{8\omega(\varepsilon_o + \varepsilon_p)(\frac{\Delta v}{v})}{3qNd\ \epsilon_s\ v^2} \left[\frac{R}{M(\ell_1/\ell)}\right]^2 [b/a]^2 \tag{21b}$$

Using the parametric circuit analysis approach, Aoki et al obtained an expression for M similar to Eq (20), if the equivalent circuit strip impedance in the acoustic beam is very much larger than the strip impedance at the semiconductor. However, if the equivalent acoustic strip capacitance is small with respect to that at the semiconductor, a new expression for M is obtained:

$$M = \frac{2\,(\Delta v/v)}{2\sqrt{2\omega}\ (\varepsilon_o + \varepsilon_p)} \left[P_{-s}(\cos\Delta)\right]^{-2} \left[\,\phi\,|\,1 + \frac{\omega c}{\Gamma}\,|^{\,2}\,\right]^{-1} \tag{22a}$$

where s is the strip periodicity, Δ is the number of strip per wavelength, c is the capacitance across the depletion layer and ϕ is the built-in junction voltage. Γ is given by

$$\Gamma = \omega k \ell b(\epsilon_o + \epsilon_p) \frac{\mathrm{Sin}(\pi s)}{\pi s} \frac{P_{-s}(\cos\Delta)}{P_{-s}(-\cos\Delta)} \tag{22b}$$

where k is the wave number. Use will be made of this equation since Γ is large for bismuth germanium oxide.

2.2 FIGURE OF MERIT FOR DEVICE EFFICIENCY

M obtained from Eq (21) is a figure of merit which is most helpful when comparing two materials combinations for convolver design applications. Another useful parameter which characterizes the efficiency of a convolution device is the bilinear conversion efficiency, F_T. Since a convolver has two input terminals and one output terminal, this efficiency is defined somewhat differently from the insertion loss characteristic of an ordinary two terminal delay line. F_T is defined as

$$F_T = \frac{P_3}{P_1 P_2} \tag{23}$$

where P_1, P_2 are the electrical input powers and P_3 is the output power into a *specified load (usually 50 Ω)*. *If* P_2 *is designated as the reference input power and* all of the power levels are given in dBm then

$$F_T(\mathrm{dBm}) = P_3(\mathrm{dBm}) - [P_1(\mathrm{dBm}) + P_2(\mathrm{dBm})]$$

and

$$\text{Insertion Loss (dB)} = F_T(\mathrm{dBm}) \cdot P_2(\mathrm{dBm}) \tag{24}$$

For example, suppose the bilinear conversion efficiency of a particular convolver is given as -60 dBm. Then, if a reference power level of +20 dBm is held fixed at one terminal, the device will have an insertion loss of -60 +20 = 40 dB. Sometimes an internal bilinear efficiency is given. In this case, the input power levels refer to the acoustic power after subtraction of the losses due to bidirectionality of the transducers and the propagation loss. Thus, $F_{T_{int}}$ is given by

$$F_{T_{int}} \triangleq \frac{P_3}{P_{1_{int}} P_{2_{int}}} \tag{25}$$

$F_{T(int)}$ can be related to the nonlinear coupling coefficient by combining Eq (25) with Eq (19). Thus,

$$F_{T(int)} = \left[\frac{M}{b}\right]^2 [R_L]^{-1} \tag{26}$$

where R_L is the output load resistance in ohms.

2.3 BANDWIDTH

The bandwidth problem for the SCC can be divided into two parts: (1) the bandwidth limitations imposed by the basic acousto-electric structure and (2) the additional limitations determined by the metallic coupling strips placed in the acoustic propagation path. These two aspects will be examined in turn.

2.3.1 Output Bandwidth for General Convolver Structure

The output of any convolver can be represented by a source voltage, V_S, (the voltage developed across the depletion layer in the silicon) in series with a source impedance, Z_S. The source impedance contains a resistive term, R_S, arising from the finite resistivity of the silicon, plus a reactive term, X_S, incorporating the capacitive reactances of the silicon, the insulating oxide layer and the piezoelectric substrate. For maximum power output at the synchronous frequency $\omega = \omega_o$ the reactive term can be tuned out with a reactive element $X_{Lo} = -X_{So}$, and the resistive load, R_L, can in theory be matched to the source resistance by means of a broadband transformer of turns ration $\nu = N_1/N_2$, where N_1, N_2 are the number of turns in the primary and secondary windings, respectively, and with ν satisfying the relation $R_S = {}^2R_L$. The basic output circuit is shown in Figure 3(a).

The power output P_o of the circuit shown in Figure 3(a) is given by

$$P_o = \frac{\nu^2 R_L V_s^2}{\left(R_s + \nu^2 R_L\right)^2 + X_{s_o}^2 \left(\frac{\omega}{\omega_o} - \frac{\omega o}{\omega}\right)^2} \tag{27}$$

With the loaded circuit Q defined as

$$Q_L = \frac{X_{so}}{R_2 + \nu^2 R_L} \tag{28}$$

the 3-dB fractional bandwidth, B, can be shown to be approximately

$$Q_L \simeq \frac{2}{B}\left(\frac{B+2}{B+4}\right) \tag{29}$$

If $Q_L = 1$, then (29) reduces to

$$B = 2/Q_L \tag{30}$$

The transformer turns ratio v required for the output network shown in Figure 3(a) is given by

$$\nu = \left[\frac{R_s}{R_L}\left(\frac{Q_o}{Q_L} - 1\right)\right]^{1/2} \tag{31}$$

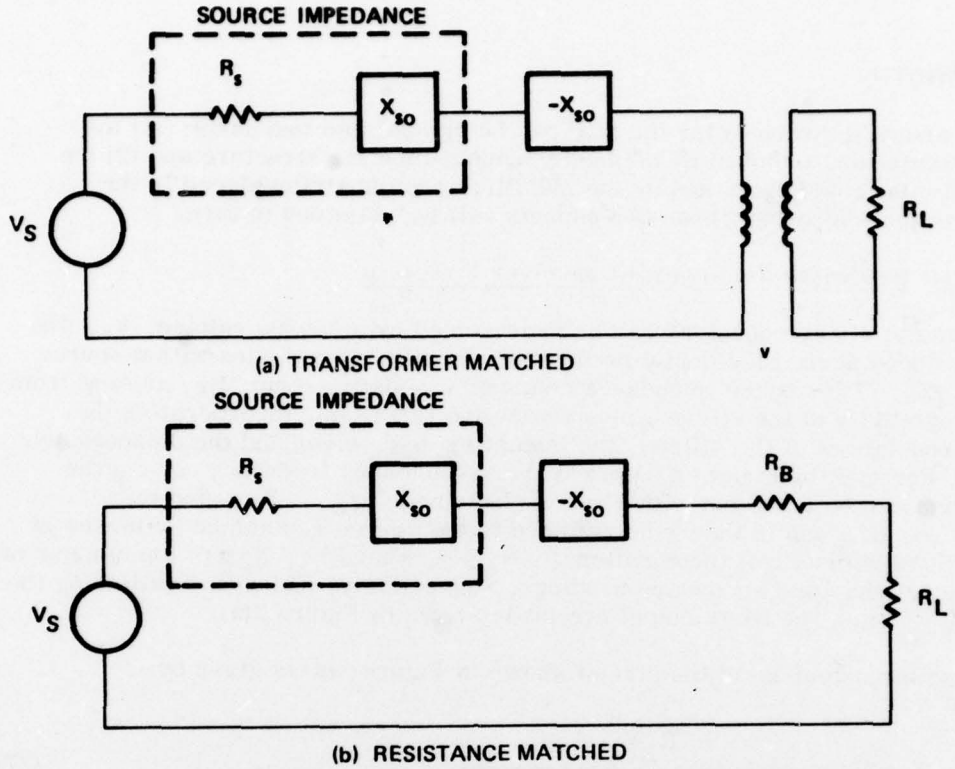

Figure 3. Equivalent Circuit, Tuned and Untuned

where $Q_o = X_{so}/R_s$ (the unloaded Q). Although possible in theory, it is not always practical to achieve the turns ratio required at the operating frequencies of SAW devices, so an output network of the type shown in Figure 3(b) must sometimes be employed. Here, the loaded Q is reduced by adding additional series resistance ($Q_L = X_{so}/(R_s + R_L + R_B)$ until the Q is small enough to achieve the desired bandwidth. Since the match is not as good for circuit b as for former circuit a, the efficiency of the network will be reduced with respect to the latter. If $Q_L{}^a$ and $Q_L{}^b$ represent the loaded Q's of circuits a and b, respectively, $Q_o{}^L = X_{so}/R_L$. Then,

$$F^a_{T(int)} = \left(\frac{M}{b}\right)^2 \frac{1}{R_s} \cdot \frac{Q_2^2}{Q_o} \cdot \left(1 = \frac{Q_2^a}{Q_o}\right) \tag{32}$$

$$F^b_{T(int)} = \left(\frac{M}{b}\right)^2 \frac{1}{R_L} \left(\frac{Q_L^b}{Q_o^L}\right)$$

Thus, while the output can be as broadband as required, some loss in efficiency will be necessary if a transformer with suitable turns is not practical.

2.3.2 Bandwidth for Strip-Coupled Structure

The large number of periodic metallic strips present on the surface of the piezoelectric substrate are a source of acoustic reflection and will thus limit the bandwidth of the device. To determine the location of the stop bands arising from this periodic structure, calculations can be made with the following approach.

The basic model employed is the standard N cascaded networks transmission matrix. This approach views the N coupling strips as N passive components, each with identical impedance Z_1 connected by a transmission line of impedance Z_2. A diagram of this system is shown in Figure 4. Physically, the change in impedance seen by the traveling SAW wave at the edge of each metallic coupling strip is due to the piezoelectric field which changes the SAW velocity by an amount v, and, to a lesser extent, to the mass loading of the strip which tends to damp out the surface wave. Referring to Figure 4, if the input voltage, V_i, and current, I_i, are known, then the voltage and current, V_o and I_o, can be calculated using the ABCD matrix:

$$\begin{bmatrix} V_i \\ I_i \end{bmatrix} = \begin{bmatrix} A_o & B_o \\ C_o & D_o \end{bmatrix} \begin{bmatrix} A_m & B_m \\ C_m & D_m \end{bmatrix} \begin{bmatrix} V_o \\ I_o \end{bmatrix} \tag{33}$$

$$= \begin{bmatrix} A_1 & B_1 \\ C_1 & D_1 \end{bmatrix} \begin{bmatrix} V_o \\ I_o \end{bmatrix}$$

where the subscripts o and m refer to the values on the transmission line (corresponding to the free piezoelectric surface), and the passive network component (corresponding to the metal strip region of the surface wave device), respectively. For N sections,

$$\begin{bmatrix} A & B \\ C & D \end{bmatrix} = \prod_{n=1}^{N} \begin{bmatrix} A_n & B_n \\ C_n & D_n \end{bmatrix} \tag{34}$$

and if each section is identical (as is the case for the metal strip structure), then

$$\begin{bmatrix} A & B \\ C & D \end{bmatrix} = \begin{bmatrix} A_1 & B_1 \\ C_1 & D_1 \end{bmatrix}^N \tag{35}$$

The A_1 B_1 C_1 D_1 values are given by

$$\begin{aligned} A_o &= \cos(2\pi f \ell_o v_o) & A_m &= \cos(2\pi f \ell_m v_m) \\ B_o &= j Z_o \sin(2\pi f \ell_o v_o) & B_m &= j Z_m \sin(2\pi f \ell_m v_m) \\ C_o &= j \sin(2\pi f \ell_o v_o)/Z_o & C_m &= j \sin(2\pi f \ell_m v_m)/Z_m \\ D_o &= \cos(2\pi f \ell_o v_o) & D_m &= \cos(2\pi f \ell_m v_m) \end{aligned} \tag{36}$$

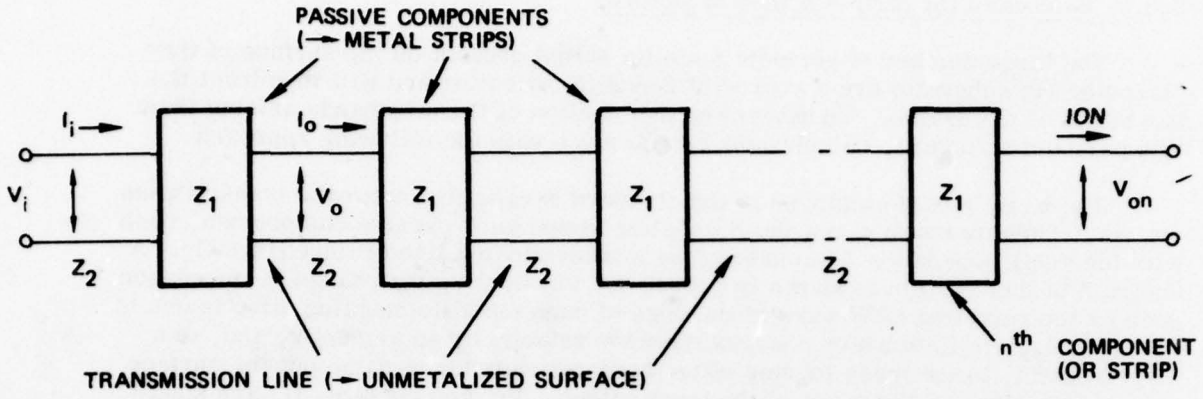

Figure 4. Cascaded Network Transmission Line

Here, f is the frequency of the SAW; v_o and v_m are the free surface and metallized SAW velocities; and ℓ_m and ℓ_o are the strip line width and gap width, respectively. Using the values of Eq (36), the $A_1B_1C_1D_1$ matrix can be calculated, and the final matrix for N strips can be determined from Eq (35). The transmission coefficient, TF (output voltage/input voltage), and the reflection coefficient, RF (reflected voltage/input voltage), can then be calculated from

$$TF = \frac{2 Z_o}{AZ_o + B + Z_o (CZ_o + D)}$$

$$RF = \frac{AZ_o + B - Z_o (CZ_o + D)}{AZ_o + B + Z_o (CZ_o + D)} \qquad (37)$$

Detailed calculations show that the values of Eq (37) are strongly dependent on Z_1/Z_2, the ratio of the free surface/metallized surface impedance; the strip periodicity, $\ell_o/\ell_o + \ell_m$; and the total number of strips, N. For a given number of strips, the strongest reflection occurs at a frequency, f_o, whose wavelength corresponds to twice the strip periodicity. This is fortunate for our purposes, since, as explained in Section 2, the strip-coupled structure must have at least three strips/wavelengths, at the operating frequency. Thus, the strongest reflection will lie at a frequency considerably above the passband of interest. Figures 5 through 7 show the reflection coefficient vs frequency for various numbers of metallic strips on bismuth germanium oxide (BGO). The strip widths are chosen so that there will be about three strips per wavelength at 100 MHz, the center frequency of the input transducer designed for this program. Note the maximum reflection in all cases occur at approximately 150 MHz, and that the reflection coefficient in the frequency range 75 MHz-125 MHz/(50% passband at 100 MHz) is always less than -30 dB. The unwanted reflection in the passband can be reduced still further by increasing the number of strips per wavelength to four (strip width = 2.1 μm). Figure 8 provides a detailed look at the 75-125 MHz region for 3,000 strips, each 2.1 μm wide. Here, the reflection coefficient is below -40 dB, except at the extreme high end of the passband.

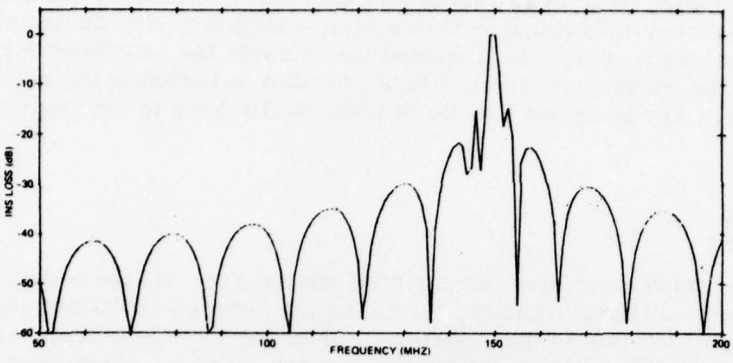

Figure 5. Transmission/Reflection Coefficient for 3,000 Coupling Strips

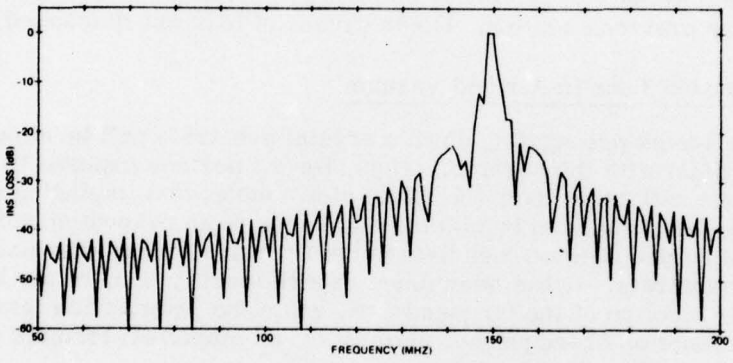

Figure 6. Transmission/Reflection Coefficients for 30,000 Coupling Strips

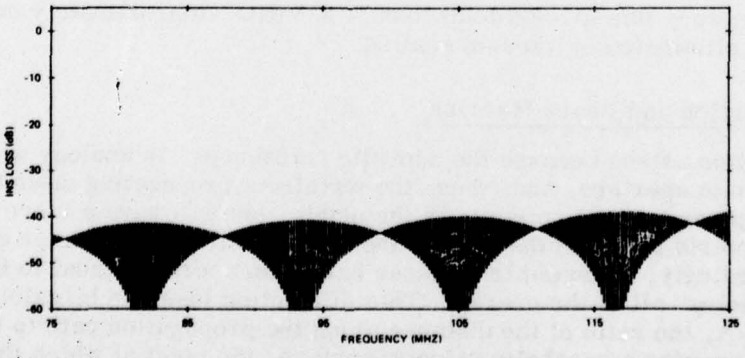

Figure 7. Expanded View of Transmission/Reflection Coefficients

The conclusion to be drawn from this analysis is that a fractional band width of 50% center frequency is obtainable with a strip-coupled device having three or more strips per wavelength, since the stopband lies outside the passband of the device. The bandwidth may be made even wider if it is possible to increase the number of strips per wavelength. Any spurious will be at least 40 dB down in the region of interest.

2.4 LOSSES

2.4.1 General

The main sources of loss for any SAW device are: (1) the 3-dB loss per transducer due to unidirectionality, (2) mismatch between IDT's and the external circuitry (sometimes this is done purposely in order to reduce triple transit), (3) beam steering and diffraction, and (4) propagation losses. These loss mechanisms have been dealt with elsewhere, and a general treatment will not be given here. The principal concern with long-delay devices are the propagation, beam steering, and diffraction losses. An additional problem with acousto-electric devices is the loss arising from the interactions of the acoustically generated electric field with the semiconductor. Reflection problems which might arise from the coupling strips were discussed in the previous section. Other causes of loss are discussed below.

2.4.2 Propagation Loss in Air and Vacuum

Acoustic waves propagating down a crystal substrate will be damped by any material in contact with the surface. Thus, for all devices exposed to the air, some propagation loss will arise from the effect of air molecules impinging on the crystal. Air loading can be eliminated by placing the device in an evacuated package, but there will still be propagation loss because of the wave energy dissipated in the lattice of the substrate. It has been found experimentally that the air loading attenuation is a linear function of the frequency, F, while the propagation loss in a vacuum is a quadratic function of frequency. For BGO, an empirical formula which includes attenuation in both air and vacuum is

$$L \cong 1.12 \times 10^{-3} F + 8.6 \times 10^{-6} F^2 \qquad (38)$$

where L is the loss in dB/cm. For our device, F (center frequency) is 100 MHz; hence, a loss of 0.198 dB/cm is to be expected. For a long interaction time of, for example, 100 μsec, this gives a total loss of 3.3 dB. Approximately one-half of this loss could be eliminated by vacuum sealing.

2.4.3 Diffraction and Beam-Steering

Diffraction arises because the acoustic transducer, in analogy with the optical slot, has a finite aperture, and, thus, the wavefront propagating down the crystal will not be a plane wave at points near the origin, but will have a more complicated pattern. At points far from the origin, the energy will spread into an even broader beam. Accordingly, an output transducer having an aperture equal to that of the input, will miss "seeing" all of the energy. This diffraction loss can be calculated as a function of X/A, the ratio of the distance along the propagation path to the transducer aperture. Assuming a parabolic velocity surface, the point at which the diffraction loss becomes equal to 1.5 dB, is given by

$$X/A = 1 + \gamma \simeq 1 \tag{39}$$

where γ is the anisotropy parameter. Thus, the diffraction loss can be made very small by proper choice of transducer aperture. For X = 16.81 cm (~100 μsec on BGO), A ≃ 83. In other words, if the total transducer aperture is 83X, the total loss due to diffraction at X = 16.81, will be ~1.5 dB.

Beam steering is a problem which can, in principle, be eliminated entirely. It arises from the fact that the acoustic beam will propagate in a direction perpendicular to the acoustic transducer only if the axis of propagation is at a certain angle, θ, with respect to the crystallographic C axis. If the propagation path is at any other angle with respect to the crystallographic C axis, the beam will veer off at an angle, ϕ, which itself changes as the orientation as $\partial\phi/\partial\phi$. In practice, there is always some beam steering, but it can be controlled so that the losses from this source will be much less than 1 dB.

2.4.4 Loss Due to Semiconductor

The presence of a semiconductor will increase the device losses because of the acoustoelectric interaction with the charge carriers and the consequent dissipation of energy by the effective semiconductor resistance R_S. An expression for the acoustic attenuation constant has been derived by Aoki et al[3]. Using the parametric circuit approach, the equivalent circuit of the nth strip is viewed as a voltage source V_n (produced by the propagating surface wave), in series with a constant reactive impedance (due to the strip on the piezoelectric surface) and an impedance consisting of a variable capacitance and a resistance (arising from the presence of the strips at the semiconductor). The attenuation constant is given by

$$\alpha \cong \frac{\sin(\pi\ell/\lambda)}{P_{-(\ell/\lambda)}(\cos \pi\ell_1/\ell)\, P_{-(\ell/\lambda)}(-\cos \pi\ell/\ell)} \cdot \frac{x \left(\frac{\Delta V}{V}\right) (\omega c)^2 R_S/\Gamma}{2\,|1 + \omega c/\Gamma|^2} \tag{40}$$

where ℓ and ℓ_1 are as defined in Section 1 and

$$\Gamma \simeq \omega k p \ell b (\epsilon_o + \epsilon_p) \frac{\sin(\pi s)}{\pi s} \frac{P_{-s}(\cos\Delta)}{P_{-s}(-\cos\Delta)} \tag{41}$$

For completeness, the expression for M given in Eqs (20) and (22a) must be multiplied by exp (-Nα), where N is the total number of strips. For gold strips on BGO having resistances on the order of 80Ω, α is on the order of 10^{-5}. Thus, for 30,000 strips, the attenuation could be increased by ~10 dB. However, if the total delay path were split into a number of channels, this attenuation would be greatly reduced; as an example, for 4,000 strips such attenuation would be only ~1.3 dB.

2.4.5 Dispersion

Because it must travel through a large number of metal strips, the velocity of the surface wave will not be constant. Further, the precise change in the velocity will depend on the metal thickness/wavelength ratio. Accordingly, for a given film thickness, different acoustic frequencies will have different propagation velocities.

This dispersion will give rise to attenuation of the wave, and this increases with the amount of metal in the propagation path. Inasmuch as a 2000:1 - 5000:1 TB strip-coupled convolver may ultimately require a total of some 30,000 metallic strips, it is most important to set limits on this dispersion loss in order to determine the maximum number of strips which can be tolerated. This loss was determined experimentally, although it can be readily calculated from known finger resistance. For the metallization represented by 4,536 strips (the number used in the SCC design), the loss was found to be about 4 dB. For 30,000 strips, the total loss would be 26 dB.

Contributions of the various loss mechanisms can now be summarized. Excluding the input transducers, the main source of attenuation for the large time-bandwidth SCC will be the metallic strips on the surface of the piezoelectric substrate. Propagation loss (air loading) with 100-μsec delays will account for no more than 3 dB; diffraction will contribute no more than ~2 dB, provided the IDT apertures are sufficiently broad; and beam steering can be eliminated by careful design. The attenuation due to metallization, on the other hand, could be nearly 30 dB, if the number of fingers required for a 100-μsec delay were deposited in one acoustic path between the two transducers. This problem is greatly reduced by utilizing the multichannel approach described in the following section.

2.5 MULTICHANNEL STRIP-COUPLED CONVOLVER

In Section 2.3.1 it was shown that, in principle at least, the SCC can have a higher bilinear conversion efficiency than the AGC, but that a serious limitation arises when it is desired to achieved long interaction times (and, hence, large time-bandwidth products) using this approach. The basic problem is that the amount of metallization required for the coupling strips rapidly becomes large enough that the increase in internal efficiency effected by the impedance is offset by an increase in attenuation in the propagating path. Also, the dispersive characteristics of the metallized surface may seriously degrade the phase coherence of the signal over a sufficiently long path. Still another aspect of the problem is that even if the signal were not impaired in any way, fabrication of a structure consisting of tens of thousands of metallic strips, each typically 2 μm less in width, would not be possible utilizing conventional photolithographic techniques. This fabrication problem is a serious drawback, since one of the supposed virtues of the strip-coupled convolver is its ease of fabrication.

2.5.1 The Solution

All of these problems can be significantly reduced by going to the multichannel approach shown schematically in Figure 8. Here, each of the input signals to be processed is divided into N parts, and each segment is fed into the appropriate IDT of one of N convolver channels. (In the schematic, each channel is a separate device, but it would be possible to combine several channels on a single substrate). Each SCC channel has the same number of strips covering 1/N of the delay between the input transducers. The number of strips employed will depend on the ease of fabrication and lack of deleterious effects on the signals. The channels are identical, except that each set of strips is located at a different point on the delay path. Collectively, the strips cover the entire distance between input IDT's. Thus, when the convolution/correlation outputs of the N channels are summed the result is identical to one channel with a prohibitively large number of coupling strips.

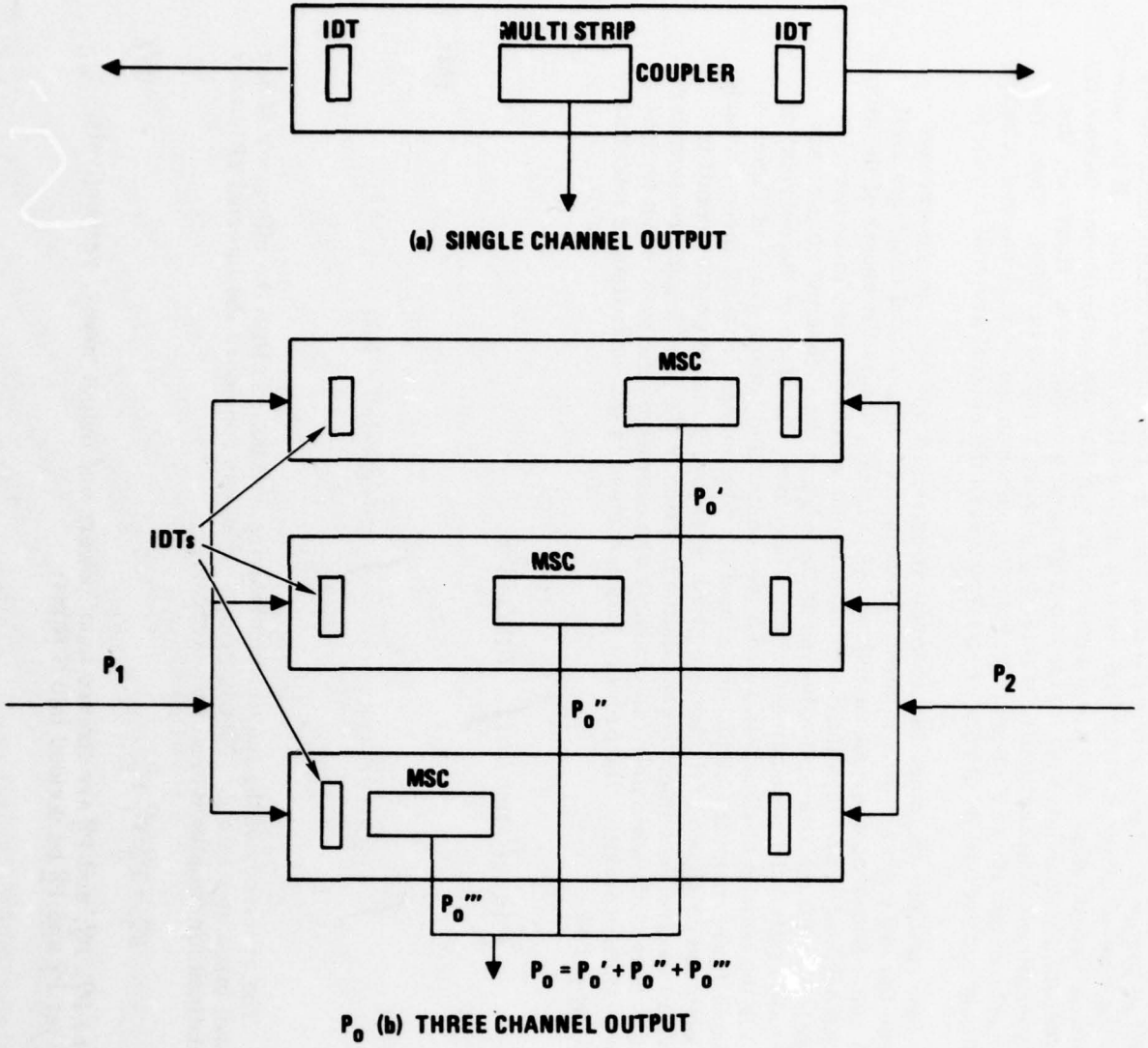

Figure 8. Multichannel Strip-Coupled Convolver

The essence of the operation of the multichannel device is illustrated in Figure 9. Three channels are shown in the diagram with transducer separation corresponding to 90 μsec. If rectangular pulses are inserted into these channels they must be 90 μsec wide in order to completely fill the interaction region. However, each set of strips on the individual substrates covers only 30 μsec of the delay. Consider two 90-μsec wide rectangular pulses fed into opposite ends of the central channel in Figure 9. Designating the time when the two signals begin interacting as t = o, the central array of strips will be completely filled after 15 μsec. If the pulses were each 30 μsec wide, this would produce the familiar diamond-shaped correlation peal, one-half of which is seen in the top-right graph of Figure 9. However, the pulses continue to interact until the total delay between inputs is filled. Thus, the convolution output for two 90-μsec rectangular pulses in the central channel (Channel 2) flattens out and will be elongated as identified in the central graph of Figure 9.

Now consider the other two channels (Channels 1 and 3). The interaction between the two pulses begins in these channels at t = 15 μsec and continues until t = 45 sec. Note that whereas the pulses began interaction in the center of the strips for Channel No. 2, and thus the convolution output reached a peak in 15 μsec, for Channels 1 and 3 the interaction begins at the edge of the strips and 30 μsec are required to fully fill the coupling region. Therefore, the slope of the correlation peak for the outputs of Channels 1 and 3 (see center and bottom graph of Figure 9) will be different from the output of Channel 2. The outputs from all three channels are combined as shown in the bottom graph of Figure 9 and in greater detail in Figure 10 to give the complete convolution function of the two 90-μsec rectangular pulses. Note that, when only two channels are operative, the sum output is non-linear. Mathematically, the process just described is the equivalent of integrating Eq (5) by parts:

$$\int_{\infty}^{\infty} f(t)\, g(\,-t)dt = \int_{-\infty}^{L_1} f(t)\, g(\,-t)dt + \int_{L_1}^{L_2} f(t)\, g(\,-t)dt + \int_{L_2}^{\infty} f(t)\, g(4-t)dt = L(t) \tag{42}$$

The efficiency of the multichannel device will be less than the efficiency of any channel taken separately. This is evident when one considers the internal efficiency F_T^o defined for each individual convolver as

$$F_T^o = P_3^o / P_1^o\, P_2^o \tag{43}$$

where P_1^o, P_2^o, and P_3^o are the two input powers and output power, respectively. Now let P_1^o and P_2^o be divided into N parts:

$$P_1^o = \sum_N P_1^o/N;\; P_2^o = \sum_N P_2^o/N \tag{44}$$

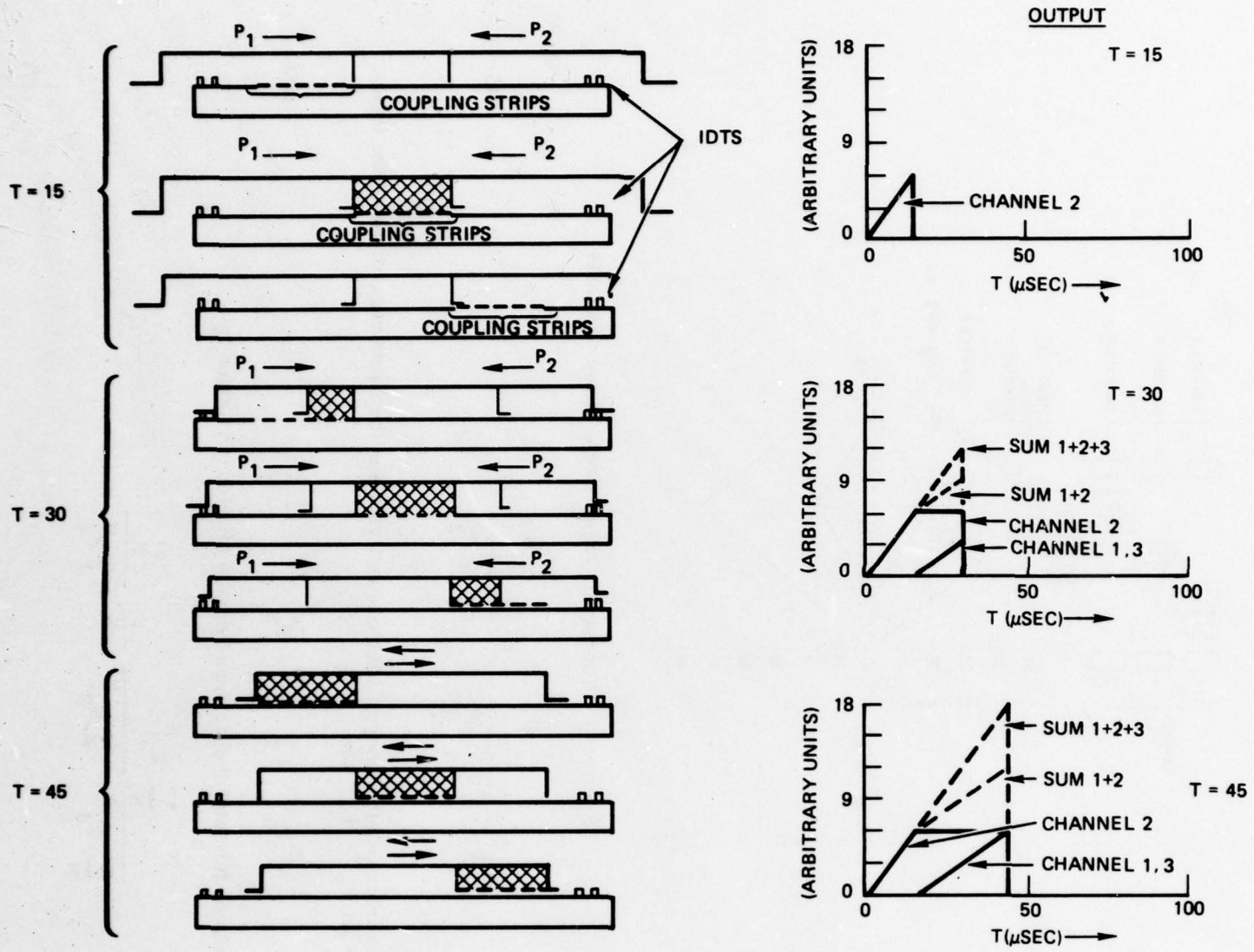

Figure 9. Interaction Mechanism for Three Channels

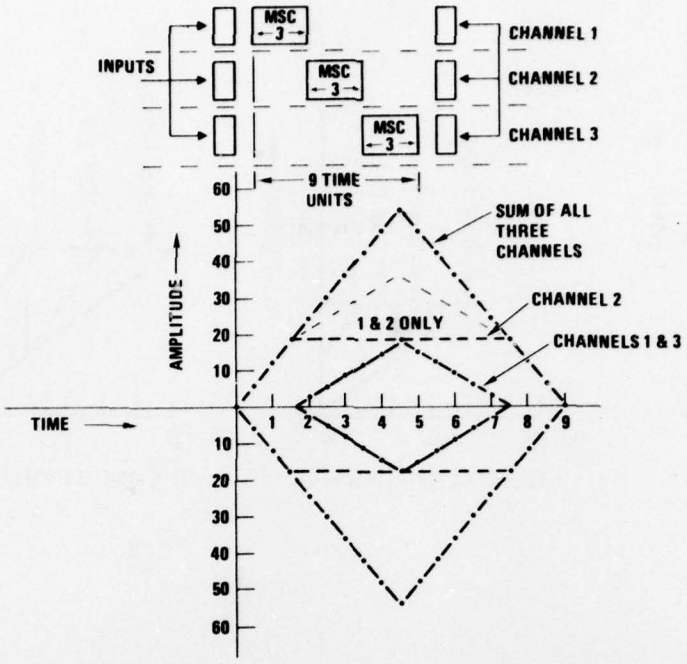

Figure 10. Convolver Output From Three Channels

$$F_T^N = \frac{P_3^N}{\frac{P_1^o}{N} \cdot \frac{P_2^o}{N}} = N^2 \frac{P_3^N}{P_1^o \cdot P_2^o} \tag{45}$$

But the internal efficiency of each channel remains the same regardless of the input power so $F_T^N = F_T^o$ and

$$N^2 P_3^N = P_3^o \quad P_3^N = P_3^o/N^2 \tag{46}$$

Therefore, the total multichannel device efficiency is given by

$$\frac{\sum_N P_3^N}{\sum_N P_1^N \quad \sum P_2^N} = \frac{1}{N} \frac{P_3^o}{P_1^o P_2^o}$$

or

$$F_{T(tot)}^N = \frac{1}{N} F_T^o \tag{47}$$

In decibel notation

$$F_{T(tot)}^{N} = F_T^{o} - 10 \text{ Log } N \text{ dBm} \tag{48}$$

Thus, for a two-channel convolver, the bilinear conversion efficiency is 3 dB less than for the single-channel device while for a three-channel device 4.8 dB are lost. However, the point to remember is that the efficiency of the SCC is some 20 dB better than for an equivalent AGC. Accordingly, with a three-channel device an improvement greater than 15 dB is obtainable and even with a five-channel model a 13-dB increase in efficiency is possible, in principle. This increase in F_T is in addition to a reduction in fabrication effort. There will clearly come a point where the fabrication of an increasing number of channels vs the drop in efficiency will render this approach counter-productive. At present, it would seem that five channels is the upper limit. How long an interaction region is achievable with a five-channel system depends on how many coupling strips can be handled by currently available fabrication techniques and/or the maximum number of strips tolerable when insertion loss/dispersion characteristics are considered.

SECTION III

DEVICE EVALUATION

The goal of this program was to develop a high-efficiency SCC with maximum interaction time, bandwidth, and time-bandwidth (TB) product. Toward this end, an SCC pattern was designed so that, when used in the multichannel system described in Section II, devices with a number of different delay times/bandwidth/TB products could be investigated. Devices representing five separate TB products ranging from 83 to 1039 were experimentally evaluated. In this section, the results of these experiments will be described. Section 3.1 presents the design approach. The materials selected for the devices and the coupling strip structure IDT patterns designed and employed are discussed in Sections 3.1 and 3.2, respectively, while the packaging for the three-channel device is described in Section 3.3. The experimental techniques and data obtained are described and discussed in Section 3.2.

3.1 DESIGN APPROACH

3.1.1 Materials

In order to obtain maximum interaction time with a piezoelectric substrate of minimum physical dimensions, bismuth germanium oxide (BGO) with a delay of 5.9 μsec/cm (001 cut, 110 propagating) was selected. In addition to having a large delay per unit length, BGO also has a relatively high piezoelectric coupling coefficient (about one-third that of $LiNbO_3$) and, hence, displays a high nonlinear figure of merit M as defined in Eq (22). However, there are two difficulties in using this material: (1) Because of the lower acoustic velocity the SAW wavelength at a given frequency is approximately one-half that on $LiNbO_3$. Therefore, photolithographic limitations on the minimum linewidth definable will dictate a lower center frequency for BGO devices as compared to corresponding $LiNbO_3$ structures; (2) since the optimum fractional bandwidth (i.e., maximum bandwidth with minimum insertion loss across the band) increases with the piezoelectric coupling coefficient, the optimum fractional bandwidth for BGO devices will be less than that obtainable with $LiNbO_3$.

As the main purpose of this program was to determine the feasibility of using the multichannel SCC approach to obtain long interaction times, it was decided that the large delay per unit length of BGO was more important than the associated drawbacks. Accordingly, an 11-in.-long, 1-in.-diameter boule of BGO grown at Rockwell's Electronics Research Center (ERC) (similar to that shown in Figure 11) was obtained. After cutting and polishing, this yielded a large number of crystalline substrates up to eight inches long. On these substrates, delays as high as 100 sec could be obtained. It is possible to achieve TB products of up to 5000 on such substrates. As discussed in Section 3.2, an easily fabricated SCC has a center frequency of about 100 MHz. A 50% bandwidth IDT at this frequency would, therefore, give a TB of 5000. However, whether this is practical depends on whether the increased efficiency of the SCC can offset the loss required to achieve such a large bandwidth on BGO; this point will be discussed in the following sections. For most of the experiments reported here, BGO bars 3.35 in. long and 0.25 in. wide were employed. Utilizing the SCC structure described in Section 3.2, delays of up to 33 μsec were obtainable, and devices having TB products of up to 1650:1 could be achieved. These

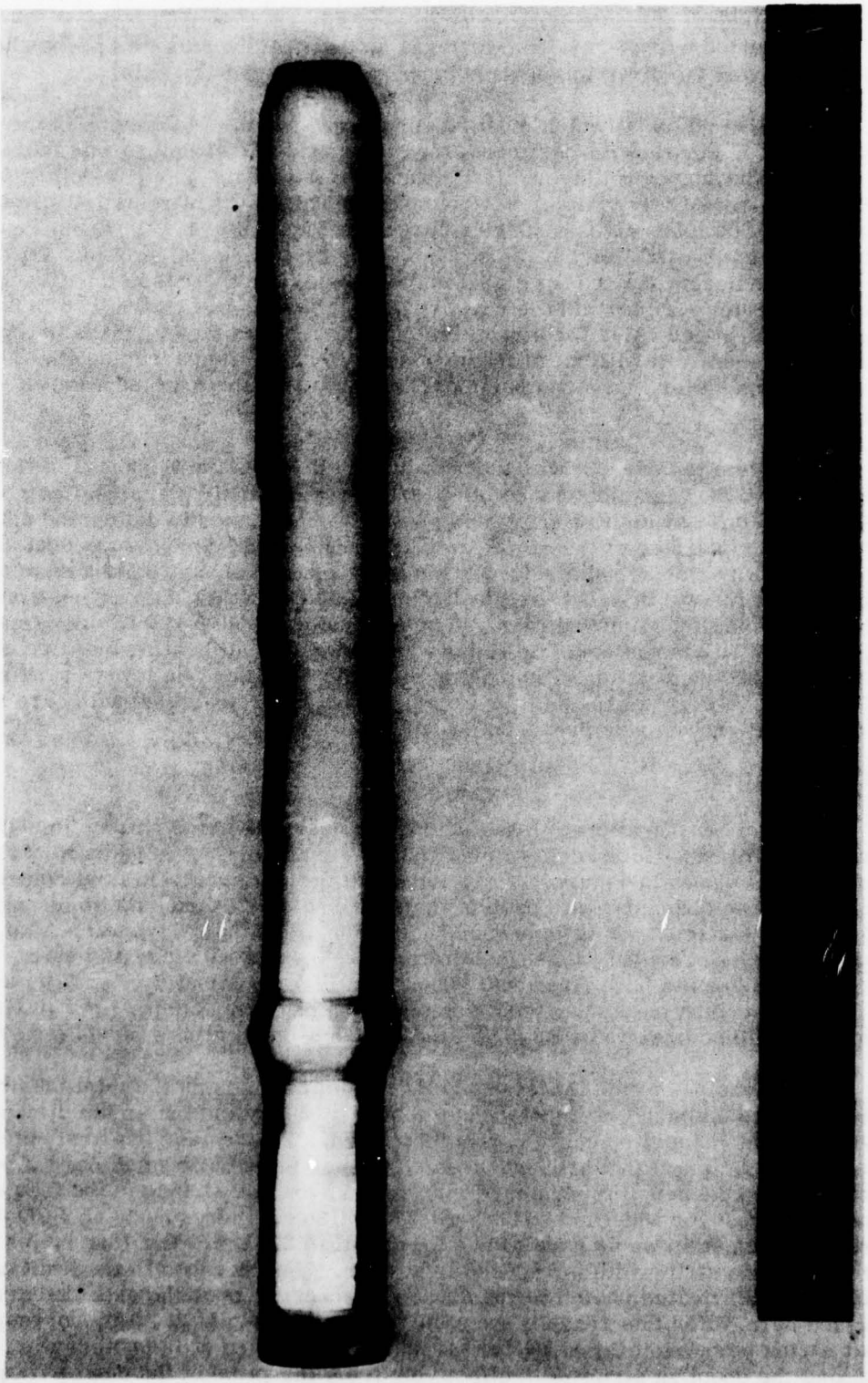

Figure 11. BGO Boule

bars were oriented with X-ray Laue patterns so that the 001 axis was perpendicular to the surface and the direction of wave propagation was the 110 axis.

The second material which must be considered for the SCC device is the semiconductor. For these experiments the semiconductor structure was fabricated from an epitaxially grown n layer on n+ silicon wafer with an impurity doping sufficient to bring the Si resistivity to about 8-10 ohm-cm. This value of resistivity, combined with a mobility of 2000, gives a carrier concentration of $\sim 3 \times 10^{14}$. From Eq (22) it will be seen that the smaller the value of qN_d, the larger the value of M. On the other hand Eq (40) indicates that a large R_S (implying small N_d) increases the attenuation constant. Previous work at this laboratory and elsewhere has shown that 10 Ω-cm is a good compromise value for structures of this type. However, there is a possibility that semiconductors with large mobilities, such as gallium arsenide (GaAs), might hold some promise for increased nonlinear interaction without an increase in attenuation.

A final item to consider with respect to the silicon is the thickness of the oxide layer, N. Because, in some modes of operation [see Eq (16)] the signal can be maximized by a specific oxide layer, experiments were performed to determine optimum h. Initially, the surface of the Si wafers used in these experiments was coated with a thermally grown oxide, 1000 Å thick. This oxide could be removed in a systematic way by etching the wafer in buffered hydrofluoric acid (HF) for a specified time period. The solution employed removed approximately 1000 Å of SiO_2 per minute; thus, a controlled amount could be removed by carefully calibrating the time of immersion. The convolution efficiency of silicon chip with oxide layers ranging from 1000 Å to zero Å were evaluated. However, the best were obtained with bare silicon (i.e., only air-grown oxide present).

3.1.2 SCC Pattern

For these investigations, it was decided to design the SCC pattern in such a way that a number of bandwidths/delay times could be evaluated. A schematic of the basic design is shown in Figure 12. As indicated in the figure, the final convolver system has three channels; with each of these channels provided with an identical coupling strip structure at the appropriate location along the delay path. Also, each of the channels is provided with three different transducers for use as inputs. The IDTs were designed to have fractional bandwidths of approximately 7%, 37%, and 50% and, thus, depending on the particular combination of IDT and delay lines utilized, the device could be operated with nine different time-bandwidth products (see Table 1).

The dimensions of the initial design were dictated by both the minimum linewidths which could be defined photolithographically and by the maximum dimensions of the mask which could be conveniently fabricated. To consider the first point, it was shown in Section II that at least three strips per wavelength (and more if possible) are required in the coupling structure in order to avoid stop bands in the frequency region of interest for wideband IDT's. At 100-MHz center frequency on BGO this means that each strip would have to be no wider than 2.8 μm. For four strips per wavelength, this strip width is reduced to 2.1 μm. This is close to the limit of what can be easily fabricated photolithographically, especially over the extended areas discussed here. For this reason, the strip width was fixed at 2.1 μm, corresponding to four strips per wavelength. (Note that this can be looked at in another way, namely, that fixing the coupling strip width effectively fixes the value of the center frequency.)

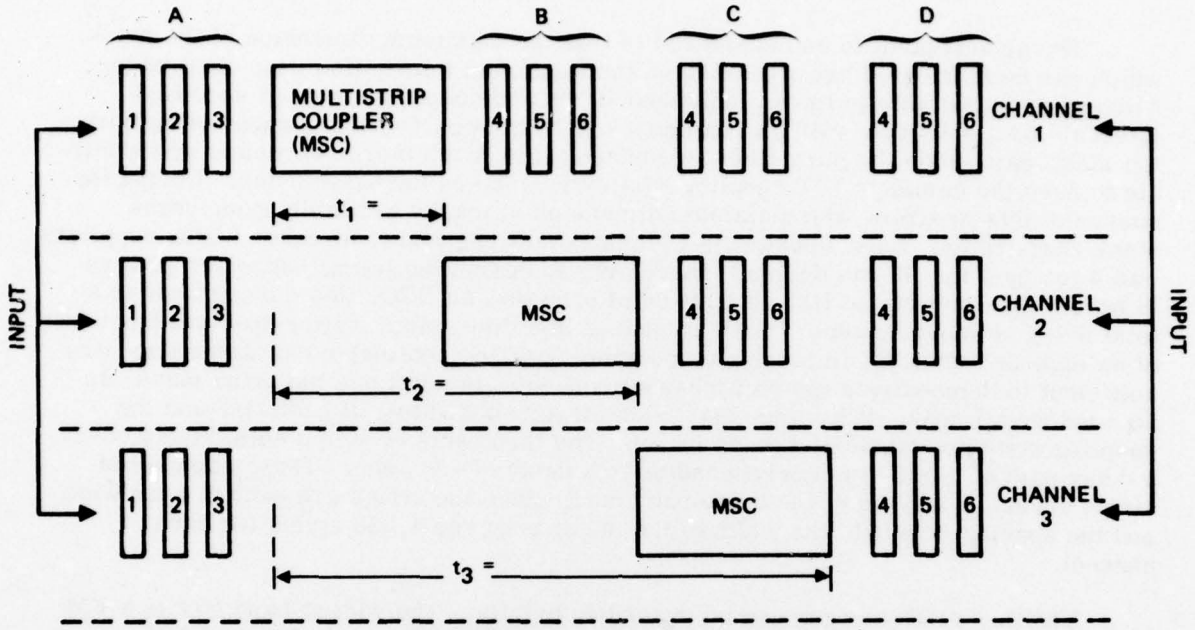

Figure 12. Multichannel SCC Design

TABLE 1. CHARACTERISTICS OF SCC DESIGN

INPUT TRANSDUCERS:

Input A	Center Frequency	BW	IDT-IDT Loss	Inputs B, C, D
1) Phase-Reversed	100 MHz	37 MHz	25 dB	4) Weighted Dispersive
2) Narrowband	100	7	10 dB	5) Narrowband
3) Weighted Dispersive	100	50	35 dB	6) Phase-Reversed

TIME-BANDWIDTH PRODUCTS OBTAINABLE WITH THREE-CHANNEL CONVOLVER:

Inputs TB	Channel 1	Channel 2	Channel 3
77	A2, B5	-	-
154	A2, C5	A2, C5	
231	A2, D5	A2, D5	A2, D5
407	A1, B6		
550	A3, B4		
814	A1, C6	A1, C6	
1100	A3, C4	A3, C4	
1221	A1, D6	A1, D6	A2, D6
1650	A3, D4	A3, D4	A3, D4

The second point to be considered is that the maximum dimension of the mask which can be fabricated has a bearing on the maximum interaction time obtainable. Although it is possible to locate individual IDT's and coupling strips at specified intervals on a substrate with an alignment machine as part of the process of defining the metal pattern on the piezoelectric surface, it is much more convenient and accurate to have the complete IDT coupling-strip structure on the same mask. During the course of this program, the maximum dimension of masks available from Trans Mask Corporation, from Rockwell's Optomask facility, and from other major suppliers was 4 in. by 4 in. It was decided, therefore, to design the initial convolver pattern to have a maximum input IDT separation of 6.66 cm; on BGO, this corresponds to a total delay of abour 40 μsec. With a mask of this dimension, a time-bandwidth product of as high as 2000:1 is, in principle, possible, and the obtainable characteristics are sufficient to demonstrate the multichannel concept. In addition, the same mask can be employed to make delay lines and much larger substrates, if each IDT and the coupling strip are fabricated individually. The three sets of strips collectively cover a delay path of 5.715 cm, corresponding to a delay of ~34 μsec. Thus, each set of strips covers 1.905 cm of the delay path, and, since the strips are each 2.1 μm wide and the spacing is equal, the width of the metal requires 4,536 strips for each channel.

The three IDT designs can be described briefly. The widest-band IDT is a FM dispersive transducer and was designed to give a full 50% bandwidth at 100 MHz center frequency. Experimental results from previous filter work has shown passbands very close to this theoretical prediction. The major drawback to the dispersive IDT is that the loss is high (estimated to be ~35 dB on BGO). From theoretical considerations, this would not be expected to pose an insurmountable problem for the MSC convolver, since nonlinear coupling efficiencies are high. However, it was expected that optimum efficiency could be obtained with two other IDT designs, and these were also available. The narrowband IDT (labeled "2" and "5" in Figure 12) was designed to have a 7% bandwidth and a theoretical insertion loss of 6 dB. Although in practice the insertion loss is about 10 dB, this design represents the maximum energy input into the SAW system. Finally, the phase-reversed (PRT) IDT (labeled "3" and "4" in Figure 12) has approximately 37% bandwidth and a theoretical insertion loss of 25 dB. The PRT is a nondispersive IDT which has a total of eight fingers, with the last pair phase-reversed with respect to the other three. This phase reversal "bucks out" one of the remaining pair, and the resulting passband is effectively that of a two-finger-pair IDT. The advantage of this design is that, when the IDT is tuned, a flat passband over about 37% fractional bandwidth can be obtained. A computer simulation of this transducer is shown both untuned and tuned in Figures 13(a) and 13(b), respectively.

3.1.3 Packaging

The package holding the three substrates was fabricated from a solid aluminum plate, measuring 3 in. by 4 in. in area and 0.8 in. in thickness. Three channels were milled in this material, to hold three BGO bars, each measuring 3-1/2 in. by 0.195 in. by 0.225 in. in size. A top view of this package is shown schematically in Figure 14. Note that for each channel sufficient connectors are provided so that any of the input transducers may be conveniently utilized. The outlets to the side of the box present no problem in this regard, since the channels are positioned conveniently near connector locations. However, for the channel in the center of the package additional channeling is required to connect the IDT's with the output terminals. To reduce

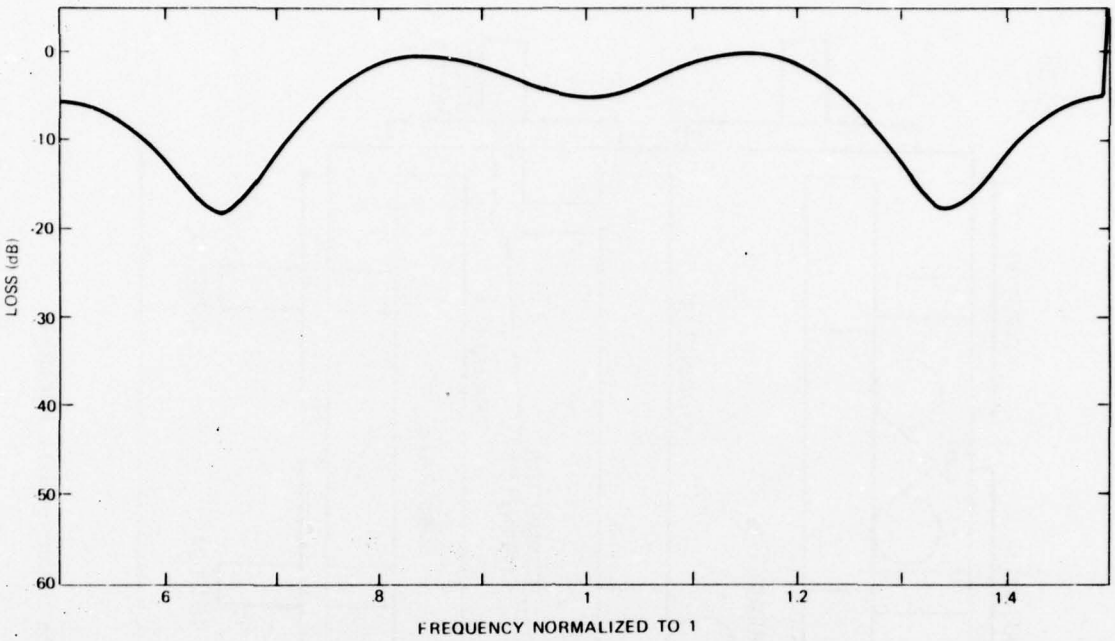

(a) PASSBAND OF PHASE-REVERSED TRANSDUCERS

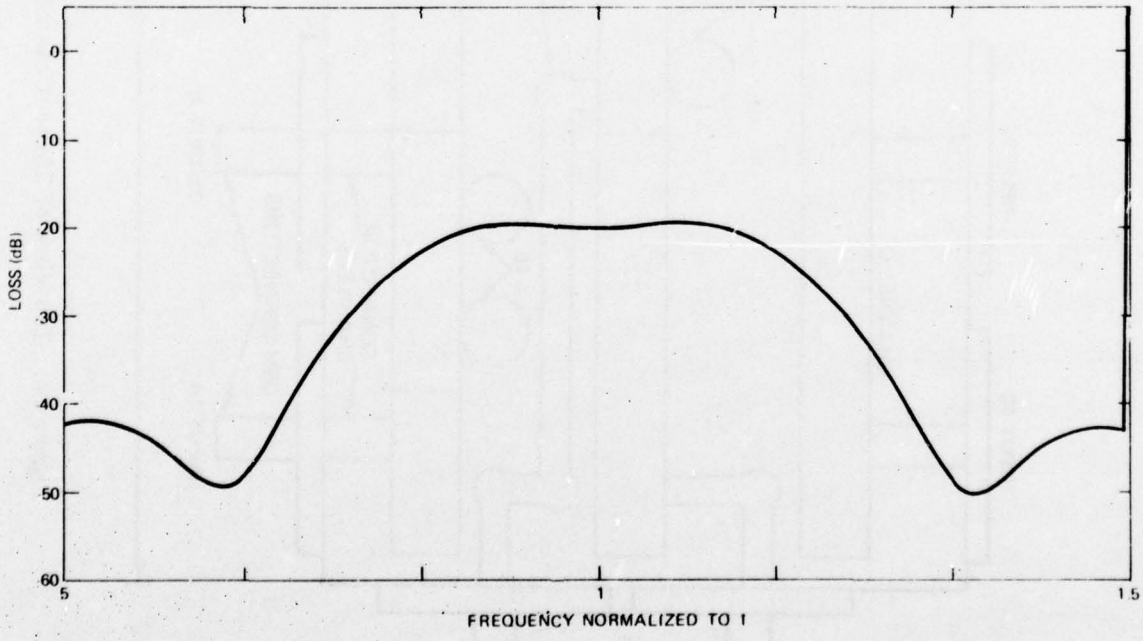

(b) PASSBAND OF TUNED PHASE-REVERSED IDT

Figure 13. Computer Simulations of Phase-Reversed IDT Passbands

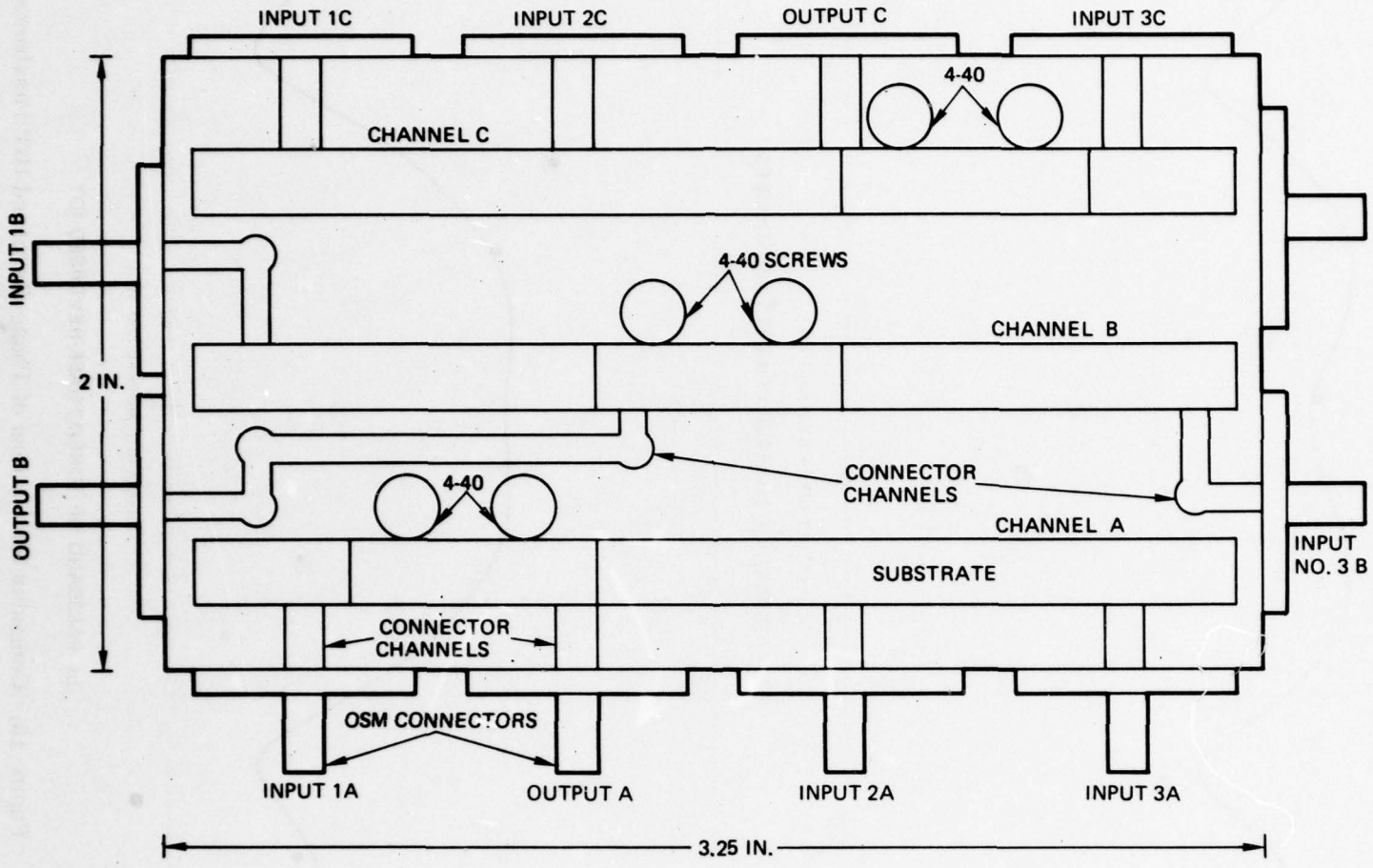

Figure 14. Top View of Three-Channel Phase-Reversed IDT Package

crosstalk which might arise from having such relatively lengthy connectors in the package, the connections from the terminals to the IDT are made with microstrip. Since the channels are buried considerably below the surface of the package, the microstrip effectively isolates competing input transducers. Note also from the diagram that enclaves adjacent to channels have been provided, so that inductors can be conveniently attached to the IDTs for tuning purposes.

In addition to the base structure shown in Figure 14, the complete package includes one additional section. The design required here is considerably more critical than for the base, since the second layer of the package is actively involved in holding the silicon chip to the surface of the coupling strips, as well as in holding partitions which provide electromagnetic isolation for the transducers. Accordingly, this second section will be discussed in some detail.

For a strip-coupled acoustoelectric device it is of utmost importance that uniform contact be maintained between the coupling strips and the semiconductor. An example of nonuniform contact is shown in Figure 38 in Section 3. In Figure 38, it can be seen that the total area of interaction is not utilized, and a signal with reduced time-bandwidth product results. The problem becomes more severe with an increasing number of strips; the 1.9-cm area covered by the strip design described in Section 3.2 is lengthy for devices of this type. The main problem here, therefore, was to devise a method for holding the silicon firmly to the coupling strips, which could also be an integral part of the package. The technique developed during this program is illustrated in Figures 15 through 17.

The first step in implementing the approach is to prepare the silicon chip. First, two ridges are etched in a rectangular silicon chip, with two ridges arranged on the surface in such a way that when the chip is placed over the coupling strips, one of the ridges will rest on the end of the strip which lie outside the propagation path, while the other ridge rests on the bare substrate (see Figure 3-16). The top of each ridge was designed to be from 3.5 μm to 5 μm above the BGO surface. One obvious problem in applying this technique is that coupling between the piezoelectrically generated electric field and the Si charge carriers might possibly take place directly across the space between the surfaces of the piezoelectric and semiconductor; indeed, this is just the mechanism for the air gap convolver. Although some air gap coupling was noted, as will be discussed in Section 3.2, the resulting signal was at most more than two orders of magnitude below the strip-coupled signal.

The method used to ensure uniform contact in the design under discussion here is shown schematically in the already referenced Figures 15 through 17, which are end, top and side views, respectively, of the silicon-on piezoelectric structure. Basically, this structure is built up in layers. First, the BGO substrate is placed into the milled channels at the base of the package. Next, the etched silicon chip is positioned on the strips, as discussed above. On top of the chip is placed a rectangle of deformable plastic having an area equal to that of the chip and a thickness of about 20 mils. A metal plate of similar dimensions is then placed on top of the plastic. At this point, the second section of the aluminum package is afixed to the top of the base; this plate is shown in the top of the photograph Figure 18. The three openings milled through it which line up with the strip-coupled structure on the substrates; through these "windows" an aluminum holder containing five 125-mil-diameter ball bearings is set on the metal plate. The ball bearings are pressed firmly against the metal plate by means of a rectangle of spring steel, which is attached to the

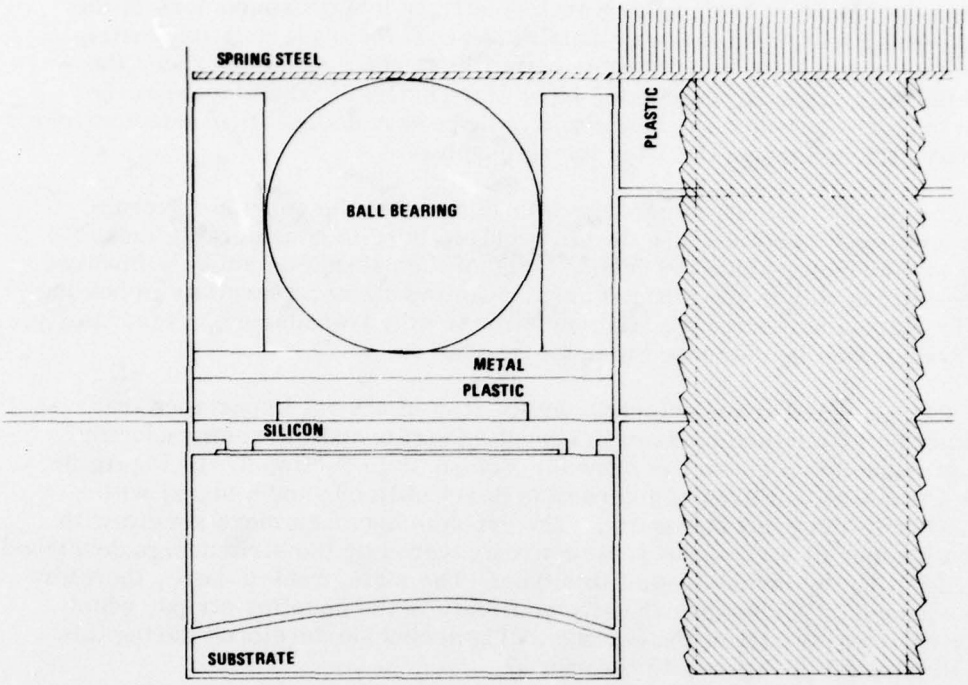

Figure 15. End View of One Channel

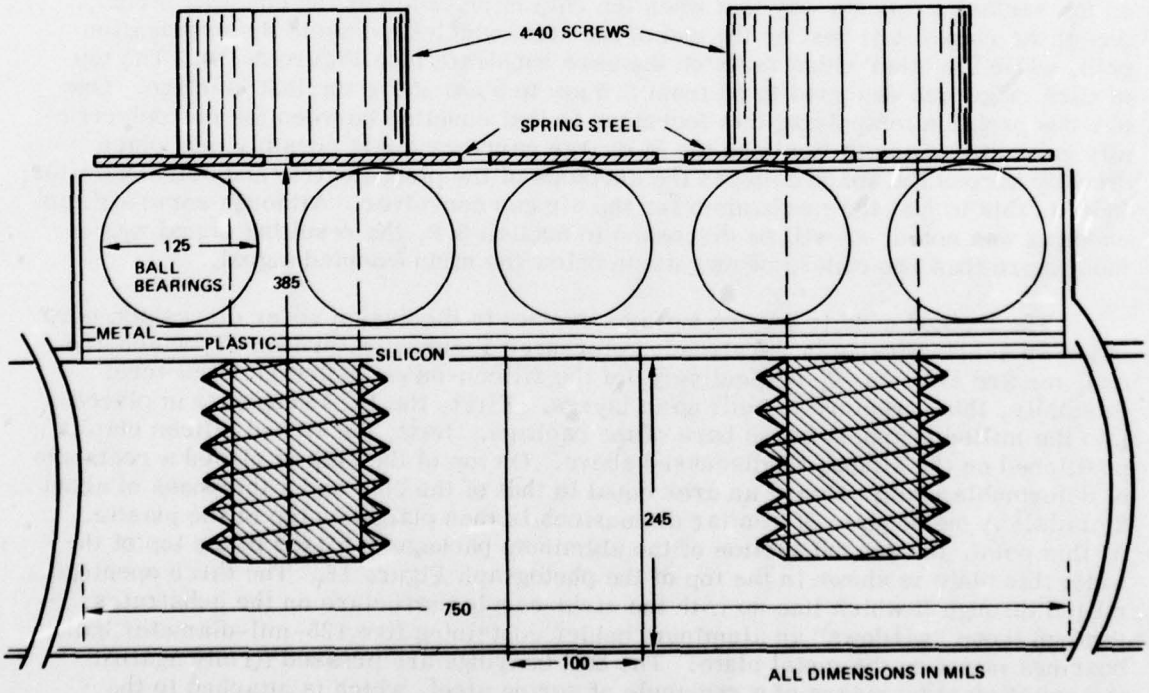

Figure 16. Side View of One Channel

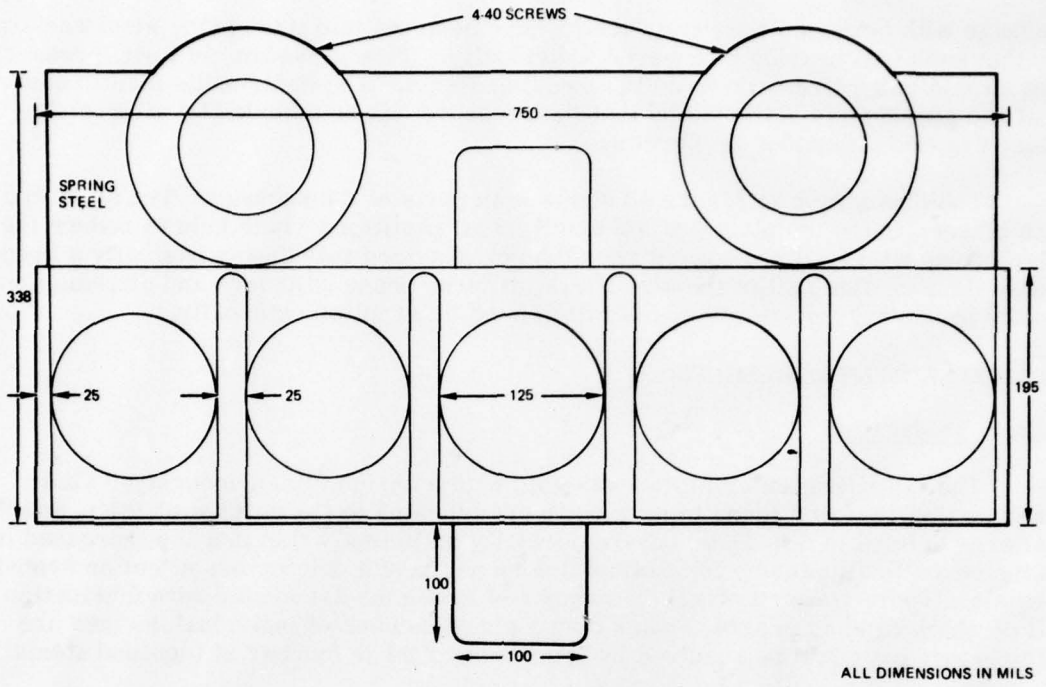

Figure 17. Top View of One Channel

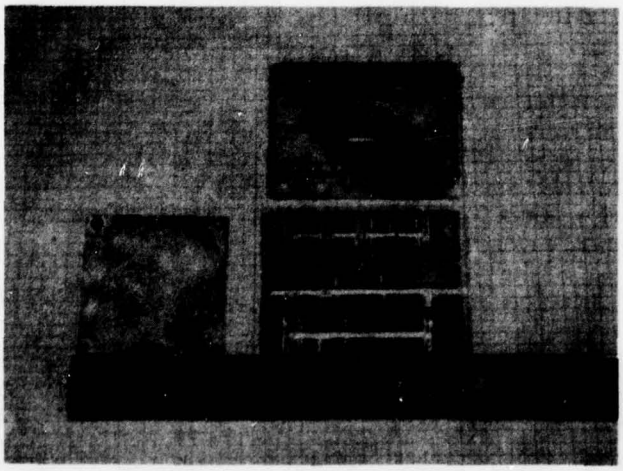

Figure 18. Photograph of Convolver Package

package with screws. Note that "teeth" have been cut into this spring steel rectangle so that each ball bearing is covered individually. This pressure, in turn, presses the silicon ridge firmly down on the coupling strips. The deformable plastic ensures that the pressure is uniform and that the pressure can be adjusted by alternately loosening and tightening the screws.

The photograph in Figure 18 shows both parts of the package. The slots that can be seen in the top plate are for small metal partitions which help to reduce the electromagnetic feedthrough. It should be emphasized that this is basically a breadboard device, since all of the amplifiers, filters, phase adjusters and attending circuitry necessary for convolver operation must be supplied externally.

3.2 EXPERIMENTAL RESULTS

3.2.1 Fabrication

The metallization employed was gold with a chrome flash underlay. This combination has been found to have optimum adhesion to the surface of BGO, and the patterns defined in this material are normally sufficiently thin that the increased mass (as opposed to aluminum, for example) does not have a deleterious effect on acoustic signals. There were, however, a number of problems associated with fabrication, all of which hamper progress when only a small number of individual devices are fabricated, but could be resolved by processing a large number of identical items.

The main problem involved the simultaneous fabrication of a large number of coupling strips (4536) having nominal widths of 2.1 μm and a number of IDT's having linewidths ranging from 3 μm to 5.6 μm. Since the IDT's were widely separated from the coupling strips (in some cases by as much as 4.5 cm) this differential in linewidth made it very important that illumination during exposure be uniform. However, a beam collimator illuminator was available which had the capability of uniformly covering up to 21 sq in. of area, and the patterns were defined on the metal without difficulty. Most of the problems occurred during the etching phase of the fabrication. The etching time required to adequately define the IDT's at opposite ends of the substrates was often found to be too long for the narrow center strips, thus removing a substantial portion of them. After a number of iterations, however, the balance between exposure time, development time, and etch time was determined and satisfactory patterns were obtained.

Since the IDT patterns were more critical than the coupling strip (i.e., the strips can tolerate a certain number of shorts, while none are allowed in the IDT's), the processing was aimed toward achieving the optimum IDT, compatible with reasonable strip definition. In most cases, this resulted in reduced strip widths. Also, in most cases, however, this presents no major problem, since the periodicity remains constant.

Another consequence of having to define a large variety of linewidths over large distances was that the final layer of metallization on the substrate tended to be quite thin, around 800 A in most cases; this introduced considerable unwanted finger resistance and, consequently, reduced the efficiency of the devices evaluated. In addition, the adherence of the metal to the substrate was not as good as is usually the case with aluminum on $LiNbO_3$ or quartz, and problems were experienced with obtaining a good thermal compression bond at the IDT pads. In most cases, however, lead

wires could be easily secured with silver epoxy, and no operational problems were identified with any metal adhesion problems.

After a number of trial runs most of the fabrication problems were solved, and those that remained were more a function of the material itself, than of any particular processing procedure. Given a large number of samples and a standardized format, these devices could be processed with high-percentage yields. For example, since exposure etch tradeoffs have now been established for devices of this type, the masks can be designed with strip widths sufficiently wider than desired, to allow for a known amount of over-etching. The ease of fabrication would be facilitated, however, if aluminum on $LiNbO_3$ was the working combination of materials.

3.2.2 Delay Line Evaluation of the Transducers

All of the transducers designed for the SCC were evaluated for passband shape, insertion loss, and ripple, by operating the devices in the delay line mode. In general, the experimental results agreed with predictions, although the losses encountered were greater than expected.

The problem common to both the narrowband and PRT transducers was a large resistive impedance component. Figure 19 is an impedance plot for a tuned 10-finger-pair IDT. In this case, the finger resistance is not severe, and the total resistive component at center frequency is 75 Ω; the Ra (radiation resistance) is 35 Ω. More typical of these transducers, however, is the plot presented in Figure 20, where the total resistive component is shown to be 120 Ω. A number of the 10-finger-pair IDT's were measured as having even higher resistance values -- some being as high as 250 Ω. An even more severe case was that of the phase-reversed IDT's; from the impedance plot drawn in Figure 21, it can be seen that the tuned impedance of these IDT's was on the order of 1000 Ω.

Much of this increase in resistance is due to the thinness of the metallization, the measured resistivity of which was 1.03 Ω/□. For the 10-finger-pair IDT having fingers λ/4 wide and 180 Ω long, this value of resistivity would give a total resistance per finger of about 800 Ω. Thus, for 10 fingers in parallel, a resistance of 80 Ω is to be expected. The phase-reversed transducer, on the other hand, has effectively only four fingers in parallel, implying a total resistance of about 200 Ω; this is less than the resistance determined from the impedance plots of the tuned IDT, but in this case, some of the total loss is due to the ferrite core in the tuning inductor. Overall, the increased resistance introduces losses into the system of up to 30 dB.

As discussed in Section 3.1, the thin metallization was mainly due to the necessity of achieving good definition for a large number of coupling strips with widths and spacings close to the limits of photolithographic technology, while at the same time maintaining equally good definition of standard IDT structures. Since only a few bars of BGO were available, a large number of devices could not be processed simultaneously, and the best samples were selected out of a relatively small number. Now that the procedures for fabrication have been established, the thin metallization should not be a significant problem for future devices.

The passbands of the 10-finger-pair (tuned), phase-reversed (untuned), and dispersive (tuned) transducers are depicted in Figures 22, 23, and 24, respectively. In all of these cases, the input and output IDT's are on opposite sides of the coupling

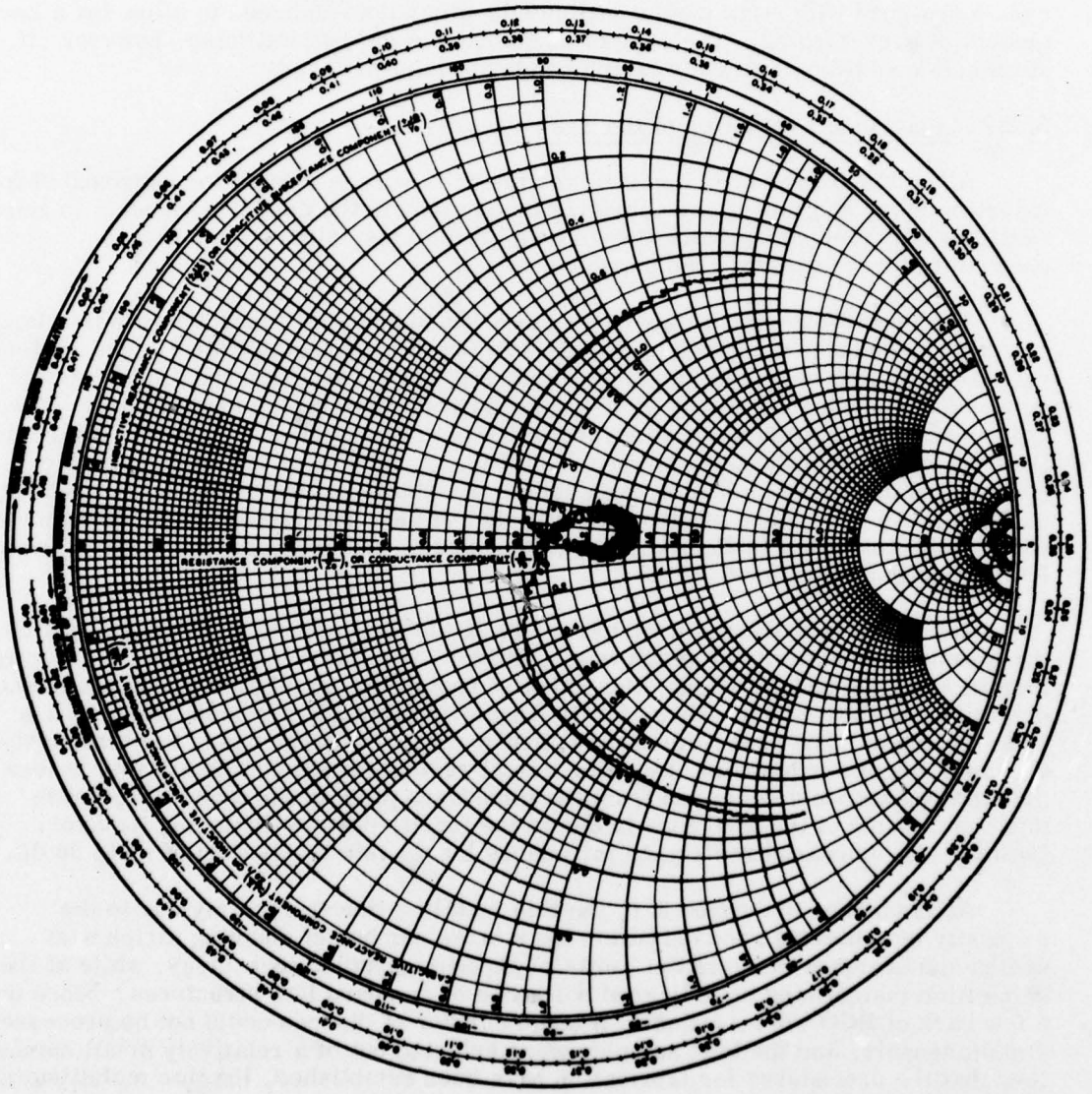

Figure 19. Impedance Plot for 10-Finger-Pair IDT; Total Center-Frequency Resistive Component, 75 Ohms

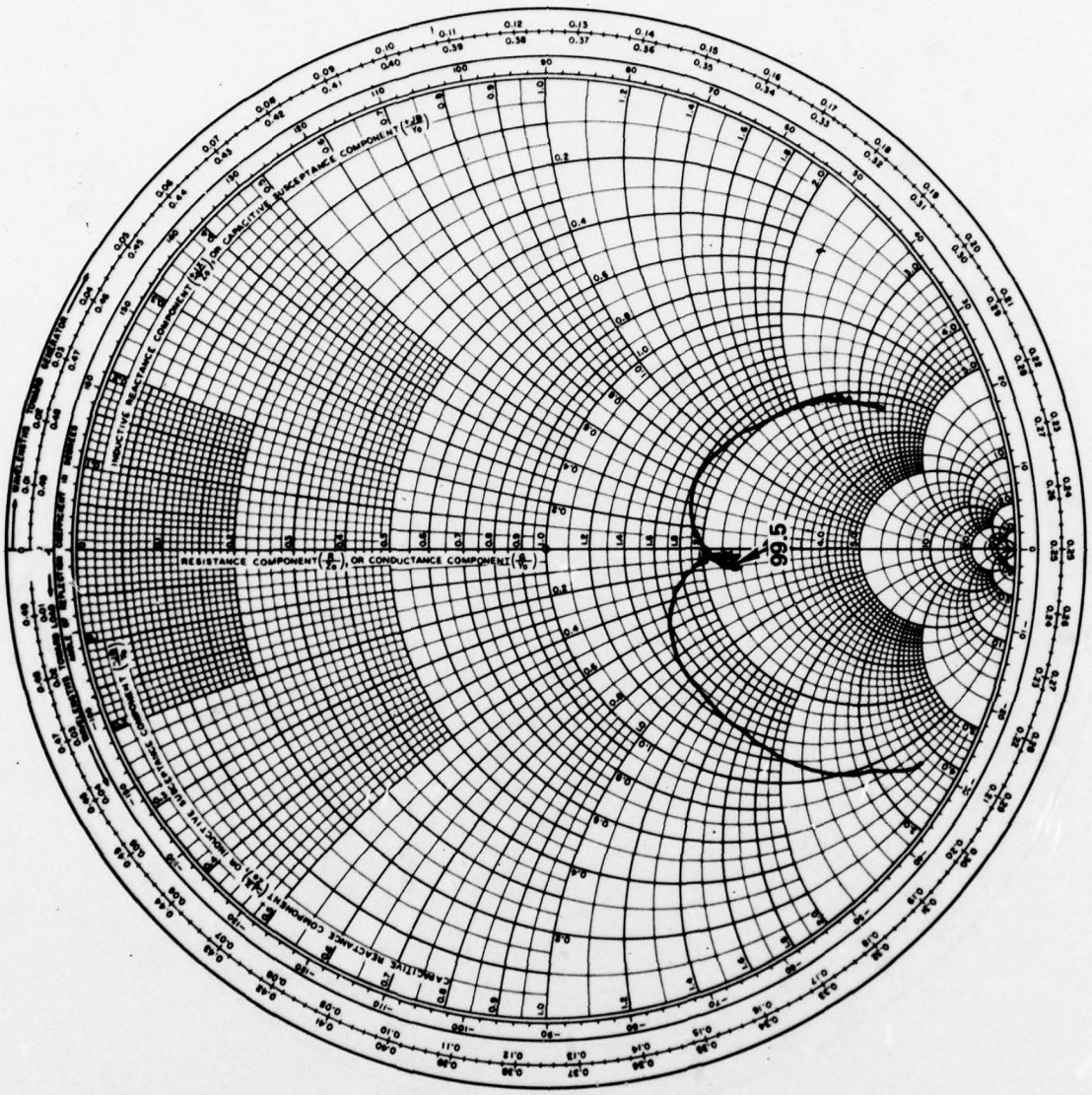

Figure 20. Impedance Plot for 10-Finger-Pair IDT; Total Center-Frequency Resistive Component, 120 Ohms

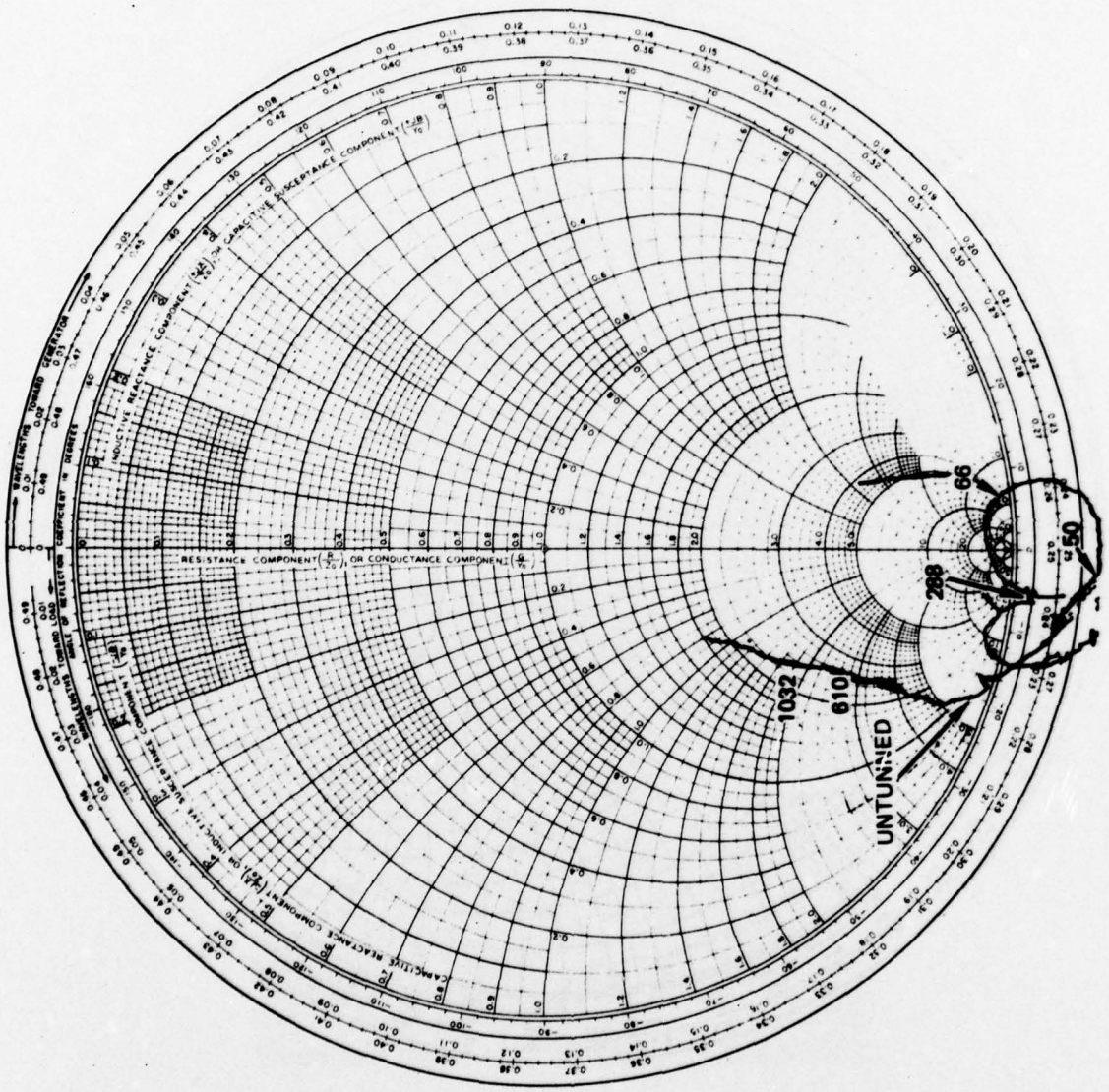

Figure 21. Impedance Plot for Phase-Reversed IDT; Center-Frequency Resistive Component, 1000 Ohms

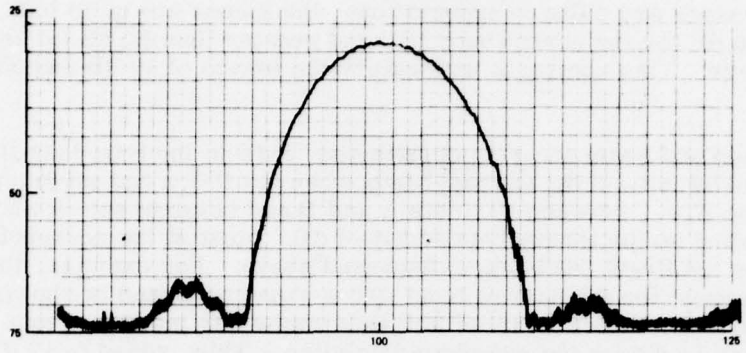

Figure 22. Transmission Plot for Narrowband IDT

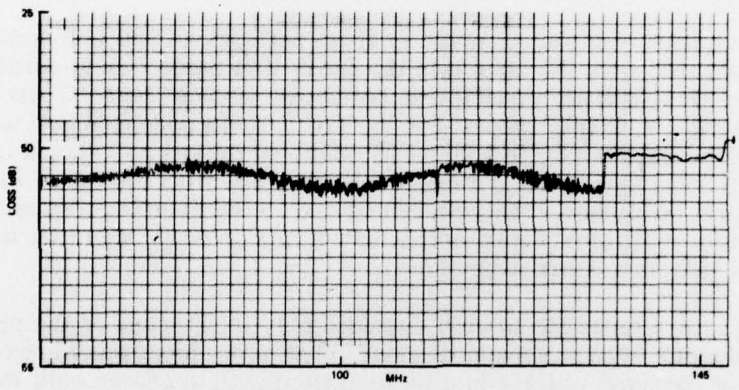

Figure 23. Transmission Plot for Dispersive IDT

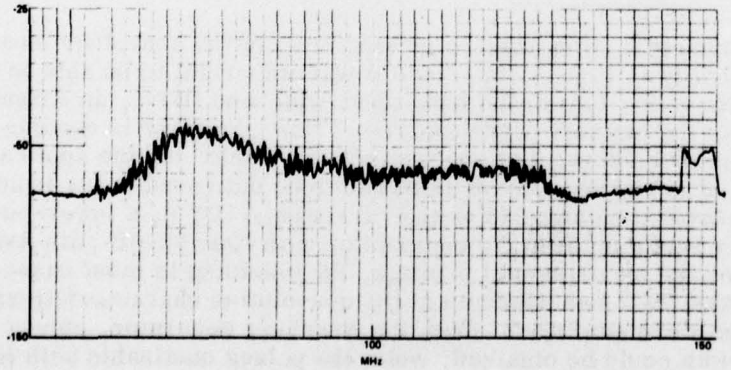

Figure 24. Transmission Plot for Phase-Reversed IDT

strips; however, all IDT's except those being evaluated have been removed. Although the passband shapes are close to expectations, the losses are quite high for all cases, being nearly 30 dB for the narrowband IDT and greater than 50 dB for the two wideband transducers. This contrasts with calculated losses of 10 dB and 35 dB, respectively.

Diffraction and beam steering contributed 2 dB to the total loss figure. This was determined by measuring the passbands when the IDT's had minimum and maximum separation (i.e., between IDT sets A and B and between sets A and D in Figure 12). The coupling strips themselves added ~4 dB. Most of the unexpected loss can be explained by the finger resistance discussed above. For example, the spurious resistive component for the narrow band IDT's whose passband is shown in Figure 24 was found to be 150Ω. With an $\hat{R_a}$ of 30Ω this implies an increased loss per transducer of 7 dB or 14 dB for the complete delay line. This, added to 12 dB plus 4 dB due to the strips, is very close to the insertion loss implied by Figure 22. The increased delay line loss reduced the convolver efficiency below acceptable levels, especially for the wideband IDT's. However, signals were still sufficiently strong to demonstrate the operational principals of the device.

Spurious signals, arising principally from reflections and bulk generations, were also investigated with the device in the delay line mode. In general, all spurious signals arising from mechanical reflection were at least 35 dB below the main signal. However, triple transit for the tuned 10-finger-pair IDT was only 17 dB below the top of the passband. In Figure 25, delayed pulses are shown in the time domain. Figure 25(a) shows the triple transit spurious with the tuned 10-finger-pair IDT, while Figure 25(b) shows the reflections due to the coupling strips. Note that in both photographs additional input-output IDT's are present, and that the reflections arising from these sources are also shown.

Bulk generation appeared to be a problem only in the case of the phase reversed transducer. The passband of the PRT at some locations showed a notch at the high end of the band which could be identified with spurious bulk modes. Bulk generation is not surprising in an under fingered IDT such as this. The effects of this spurious could be greatly reduced by roughing and/or beveling the back surface of the substrate.

3.2.3 Convolver Measurements

The experimental setup used in making most of the convolver measurements is shown schematically in Figure 26. Since it was important to be able to deliver large amounts of power (~20 dBm) to the high-loss, wideband IDT's, an Arenburg generator was employed as the primary signal source. This generator is capable of delivering 5 watts to a 50Ω load and was, of course, heavily padded for the application reported here; however, it permitted maximum power to be delivered to the input transducer in an easily controlled manner. For the narrowband IDT's, a lower-power HP608C signal generator was employed, in conjunction with two +28-dB-gain Avantec amplifiers. For the experimental package, the shielding in most cases was not sufficient to make CW measurements of the convolution characteristics; therefore, pulse techniques were employed. With the Arenburg generator, pulses from 10 μsec to 30 μsec in width could be obtained, while the pulses obtainable with the HP608C were up to 100 μsec wide.

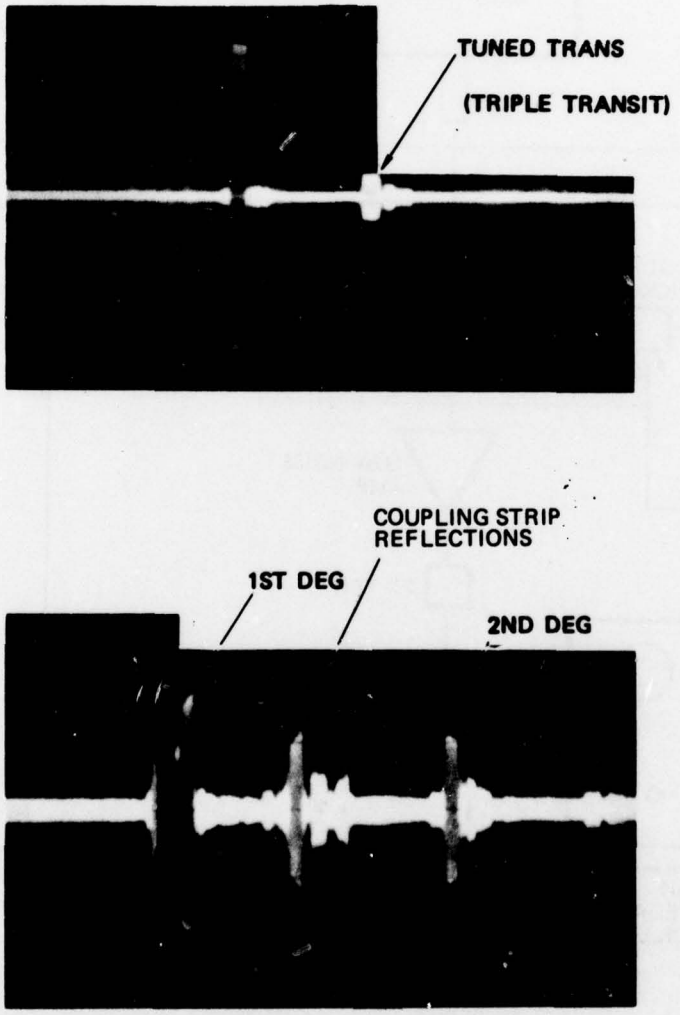

Figure 25. Reflections Present in Time Domain

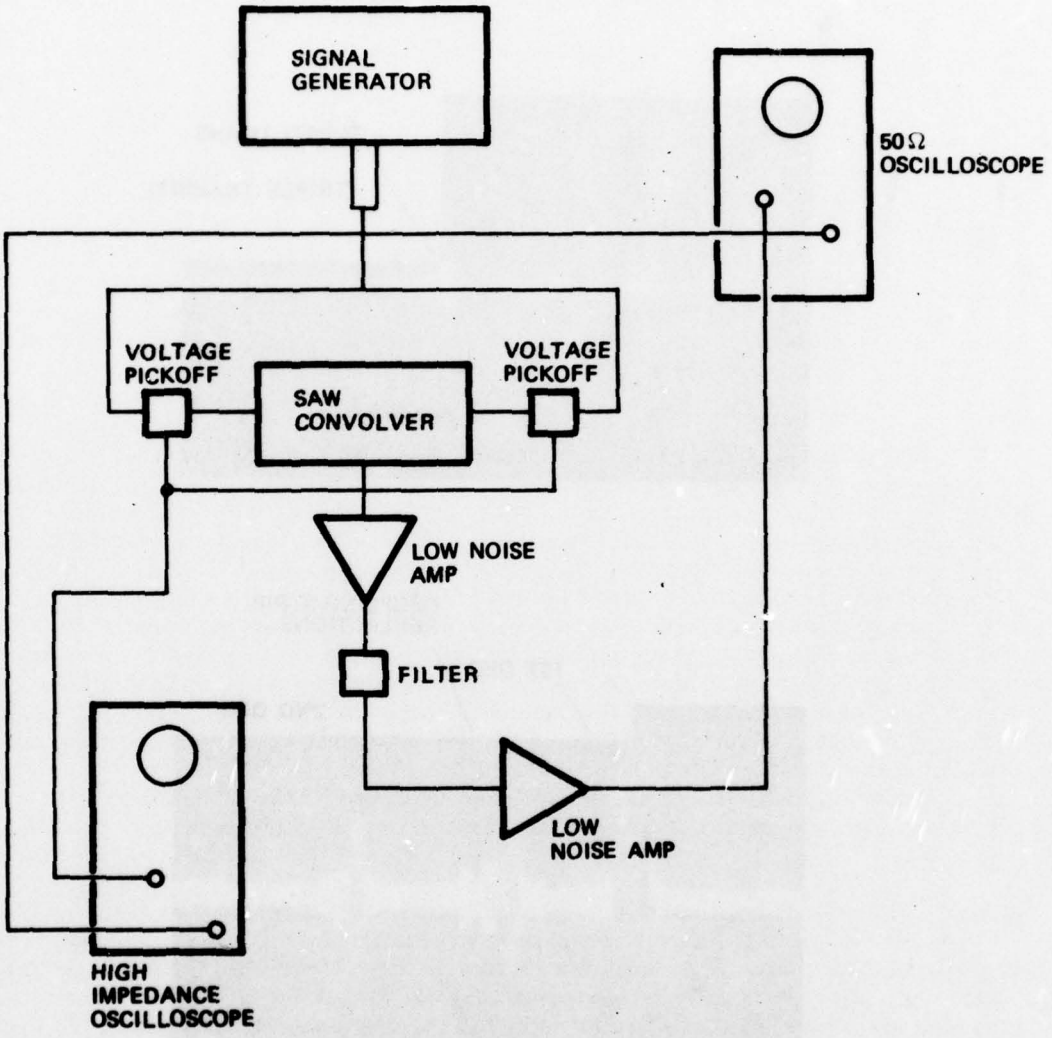

Figure 26. Apparatus for Convolution Measurements

Measurements were made with strip-coupled convolvers consisting of one, two and three channels. The bandwidths of these devices varied from 7.4 MHz to 46 MHz, while the interaction lengths were from ~11 μsec to ~33 μsec. In the discussion that follows, the designations of the three convolver channels will be taken from the diagram shown in Figure 12; i.e., the channel with the coupling strips centered between the two input IDT's will be referred to as Channel 2, while the upper and lower channels in Figure 12 will be referred to as Channels 1 and 3, respectively.

A typical one-channel convolver output is shown in Figure 27. Here, the two-input IDT's had identical 7.4-MHz bandwidth and the interaction region covered 113 sec; therefore the time-bandwidth product of this device is 83.6. Data for this device are given in Figure 28, where electrical output power (i.e., the power dissipated across a 50 Ω load) is plotted vs power dissipated across the Ra for one IDT. For this single-channel device, the internal bilinear conversion efficiency F_T = -42 dBm. Note that this is internal F_T and is determined by considering only the input power dissipated by the radiation resistance and subtracting all additional losses. Including all losses, the total F_T = -72 dBm, which is close to the figure of merit being obtained with $LiNbO_3$ AGC devices. The loss due to thin metallization and mismatch amounted to 15 dB for this device. If the resistive losses could be eliminated the device would, therefore, have an overall efficiency of -57 dB, a substantial improvement over airgap devices.

Figure 29 shows the outputs of Channels 1 and 2; note that the photograph of Channel 1 output has a scale of 10 μsec/div and the signal appears 113 μsec later than the output signal for Channel 2. The sum of the outputs of Channels 1 and 2 is shown in Figure 30. It will be seen that, as was pointed out in Chapter II, the sum is octagonal in shape. It would be easy, by proper gating of the input signals, to eliminate the nonlinear feature and to obtain simple two-channel operation. The principal difference between one- and two-channel operation is that the phase relationships of signals at both the inputs and the outputs are very important. The main problem at the input is to ensure that signals of equal magnitude are fed into the convolver channels. For the two-channel devices, it was found that this problem was effectively solved by using coaxial cables of identical length for inputs into the four terminals. These inputs were monitored by placing Textronic CT-13 signal pickoff devices at each input terminal and displaying the signal on a high-impedance oscilloscope. By keeping all of the cables equal in length, the inputs could be kept equal within less than 0.1 dB.

The phasing problem is more complicated at the outputs of the device. Here, if there is any deviation in either phase or frequency between two signals the resulting summation will be distorted or nonlinear, and output with reduced amplitude (or with zero amplitude if the out-of-phase signals cancel) will be produced. An example of slight distortion due to phase difference is shown in Figure 31. Note the difference in edge linearity for the sum signals compared with that of the signal shown in Figure 30. For the experiments performed here, it was found that the proper phasing could be obtained by using varying lengths of cables at the outputs, and, most importantly, by using a line stretcher in the individual arms. By noting the effect of the line-stretcher adjustments on the output, it was determined that a phase difference of about one part in 100 would measurably degrade the slope of the sum signal. It is likely that the phasing requirements would be even more stringent on phase-coded waveforms. It is important to note that the phase differences need not arise from the summation technique used. If the velocities are different on each

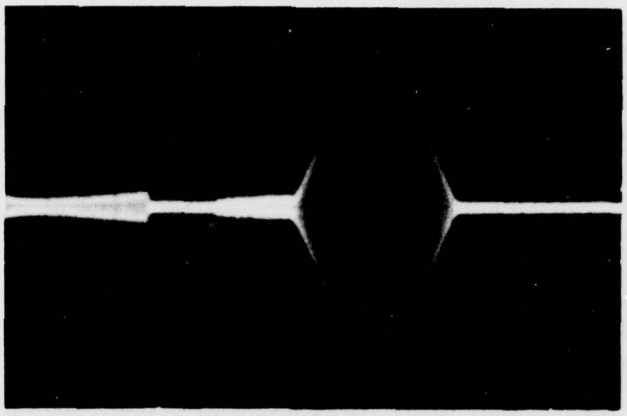

Figure 27. Convolution Output of Single-Channel (7.4-MHz Input Bandwidth)

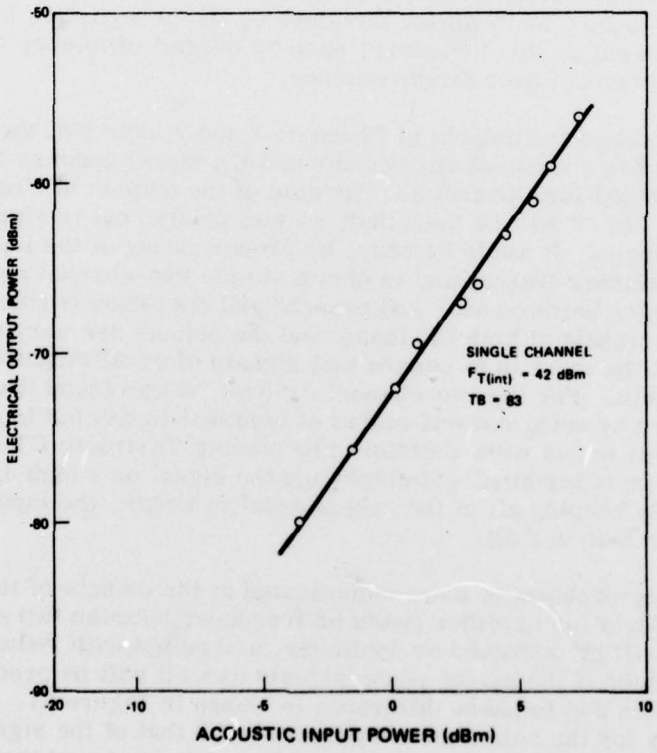

Figure 28. Acoustic Power Input to the IDT's vs Electrical Output Power for Single-Channel Narrowband Convolver

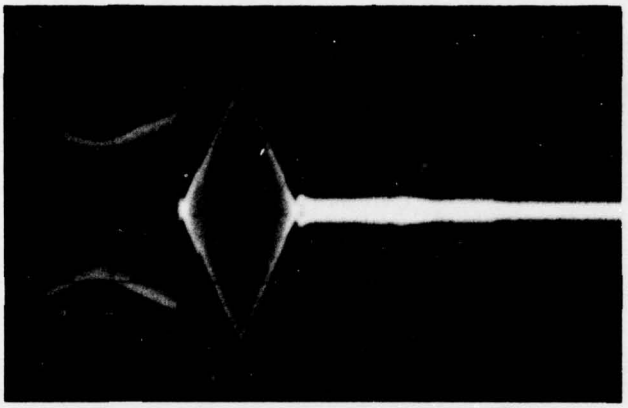

OUTPUT CHANNEL NO. 1
HORIZONTAL SCALE - 10 μSEC/DIV
VERTICAL SCALE - .02V/DIV

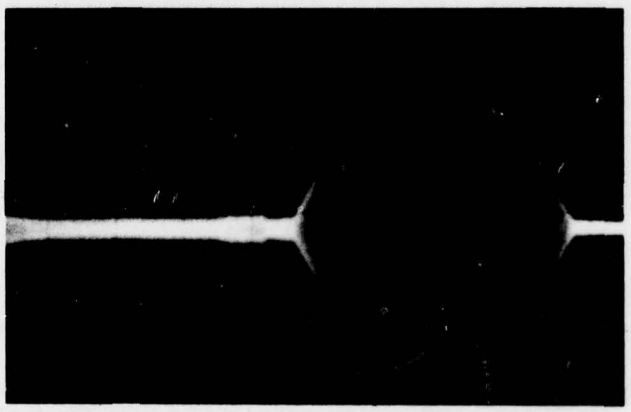

OUTPUT CHANNEL NO. 2 (CENTER)
HORIZONTAL SCALE – 5 μSEC/DIV
VERTICAL SCALE - .02V/DIV

Figure 29. Convolution Output of Two Channels (7.4-MHz Input Bandwidth)

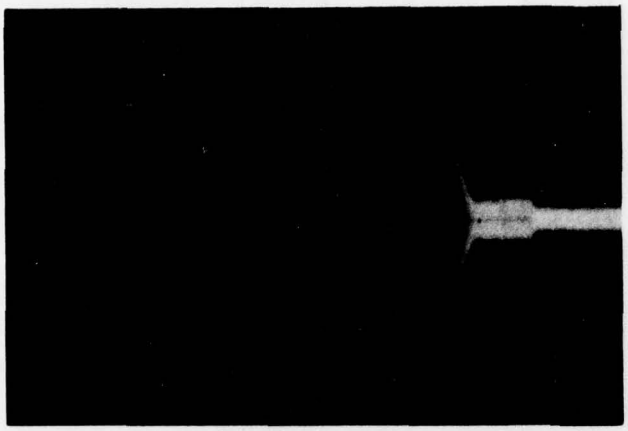

SUMMED OUTPUT
CHANNEL NO. 1 AND CHANNEL NO. 2
HORIZONTAL SCALE – 10 SEC/DIV
VERTICAL SCALE – .02V/DIV

Figure 30. Summed Output of Two Channels

substrate, as might arise, for example, if slight error in alignment of the pattern on the crystalline surface were made, then the phasing at the output will vary with time and a beating phenomena will occur. This was not observed, however, in the experiments performed here. The line stretcher and variable length cables were sufficient to obtain a satisfactory sum output.

The external output power vs acoustic input power per channel for one- and two-channel devices measured under identical conditions is shown in Figure 32. Note that separation of the two lines is ~3 dB as expected for two channels. The external F_T for the single channel here is ~ -81 dBm.

A three-channel summation (still with 10-finger-pair IDT's) is shown in Figure 33. The resistive losses in these input transducers were especially large ($R_S \simeq 250$), and the total efficiency was decreased accordingly to ~-106 dBm. Nonetheless, the three-channel summation having a total TB of 250 was achieved.

Results with the wideband transducers are shown in Figure 34. These data were taken with the dispersive transducers at the inputs. Because of the 47.5-dB loss with these IDT's, the total F_T was quite low. However, we were able to demonstrate wideband convolution response with these IDT's, and to show that no stop bands are present over the ~46-MHz range investigated. The difference between $F_{T(int)}$ for the one-channel devices and the two-channel device is about 8 dB or 5 dB greater than expected. This is largely due to the fact that contact problems prevented the complete strip structure from being utilized in one channel.

As can be seen from Figure 25, the passband of the dispersive IDT is not uniform and falls off at the high-frequency end. However, the delayed signal is quite flat across the band as shown in Figure 35, and the convolution output follows the passband reasonably well as is shown in Figure 36. It is in this sense that we say that the TB's of these devices correspond to 519 and 1039, respectively, although the passbands are not measured from 3 dB points.

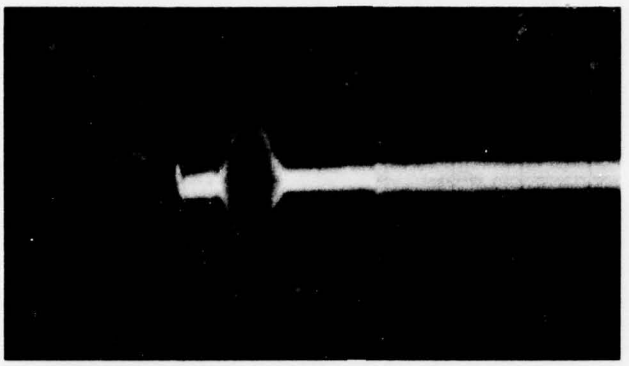

(a) CHANNEL 1

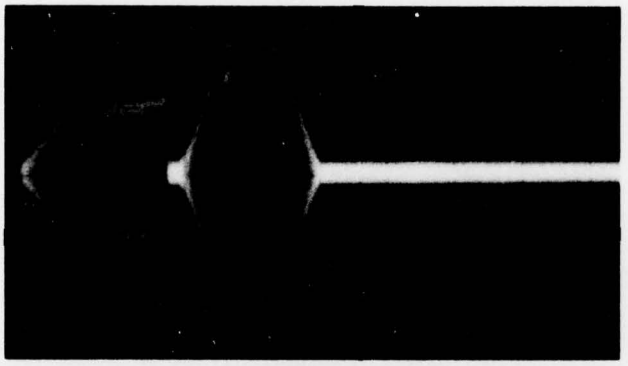

(b) CHANNEL 2

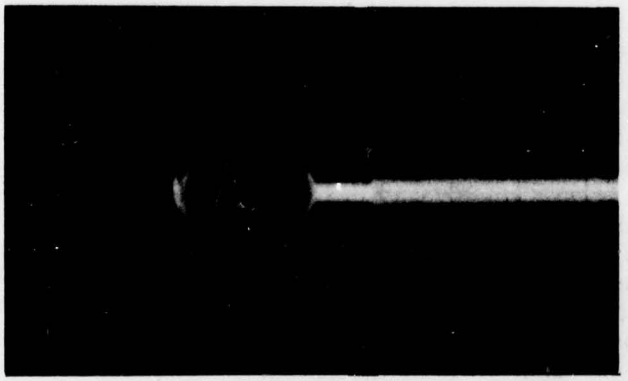

(c) CHANNELS 1 AND 2

Figure 31. Two Outputs and Their Sum

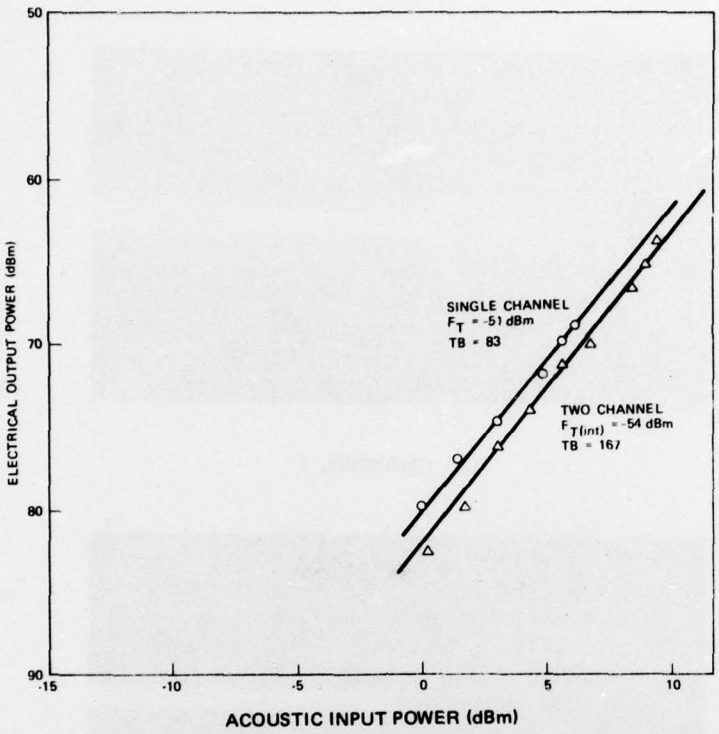

Figure 32. Acoustic Power Input to the IDTs vs Electrical Output Power for One- and Two-Channel Operation

Data for all convolvers evaluated are summarized in Table III. 2.

Two main problems with this convolver design unrelated to the IDT finger resistance problem discussed above. The first and least serious of these problems concerns the direct interaction of the propagating waves across the air gap. The surface of the silicon was at least 3.5 μm above the piezoelectric material and was 5 μm above it for one design. From calculations using Eqs (22) and (28), one would expect a nonlinear coupling coefficient M on the order of 10^{-5} volt/m/watt for separations of this kind, corresponding to an F_T at least five orders of magnitude below that expected for the SCC. In Figure 37(a), convolution output (wideband IDT's used) is shown when the Si chip is placed in the surface of the piezoelectric material without pressure applied from the spring steel. Figure 37(b) shows the convolution output when firm contact is made between the silicon and the strips. This latter signal is ~21 dB above the direct-coupled output. The discrepancy between measured and calculated values for the SCC can be best explained by the contact problem discussed below. The air gap effect could be eliminated entirely by coating the silicon surface over the piezoelectric material with a thick oxide layer (~1000 A), by changing the packaging design so that the silicon does not span the crystal surface, or by increasing the spacing substantially (i.e., from 5 μm to 25 μm).

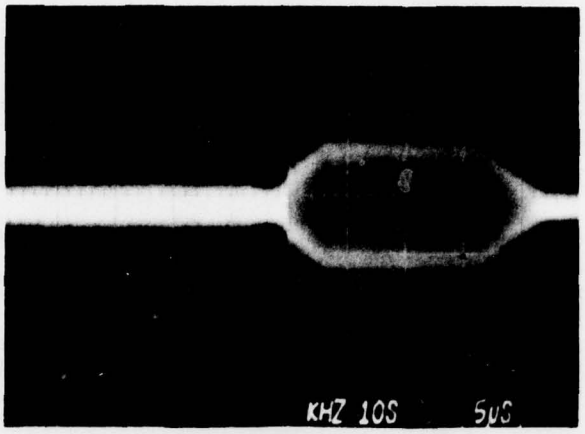

(a) CHANNEL 2

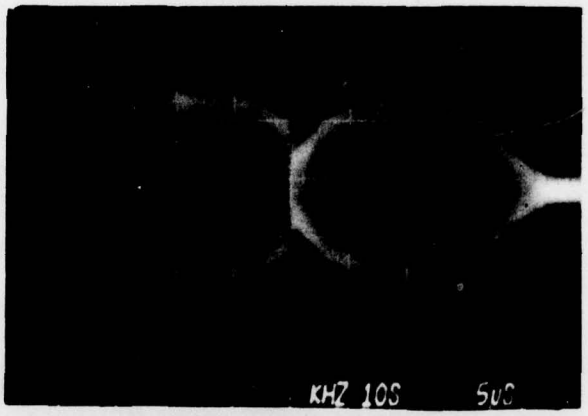

(b) CHANNEL 2 AND CHANNEL 1

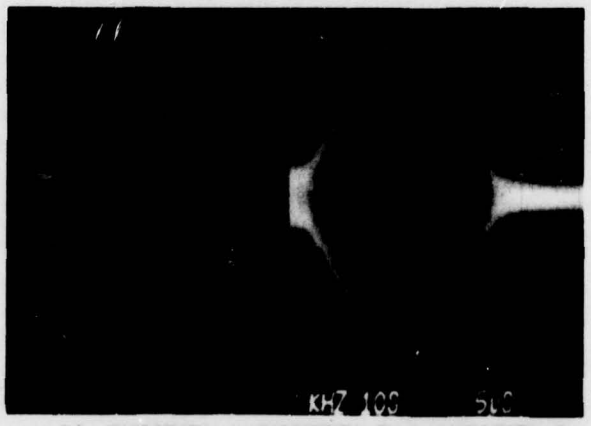

(c) CHANNEL 1, CHANNEL 2, & CHANNEL 3

Figure 33. Outputs and Sum of Three Channels

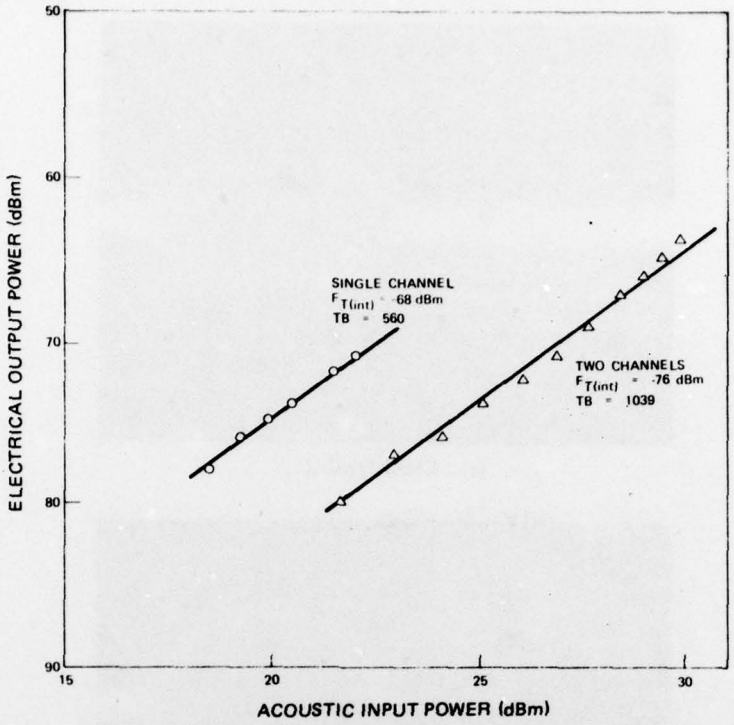

Figure 34. *Acoustic* **Power Input to the IDTs vs** Electrical Output for One Channel

The more serious problem is the fact that the silicon ridge must be maintained in firm, uniform contact throughout the extent of the coupling strips. If uniformity is not maintained, the interaction region will not be filled and, as a consequence, a signal with reduced TB will result. An example of this is shown in Figure 38(a), and the summation of one such signal with one of a different width is shown in Figure 38(b). This problem caused a great variation in the internal efficiencies listed in Table 2. The spring steel-ball bearing system was designed to ensure uniformity, but there were problems in maintaining uniformity over the 1.9 cm required. To solve the problem, a new mechanical arrangement could be designed so that adjusting screws were on both sides of the chip, rather than on just one side as is true for this model (see Figure 12). Another possible solution to this problem is discussed in Section IV.

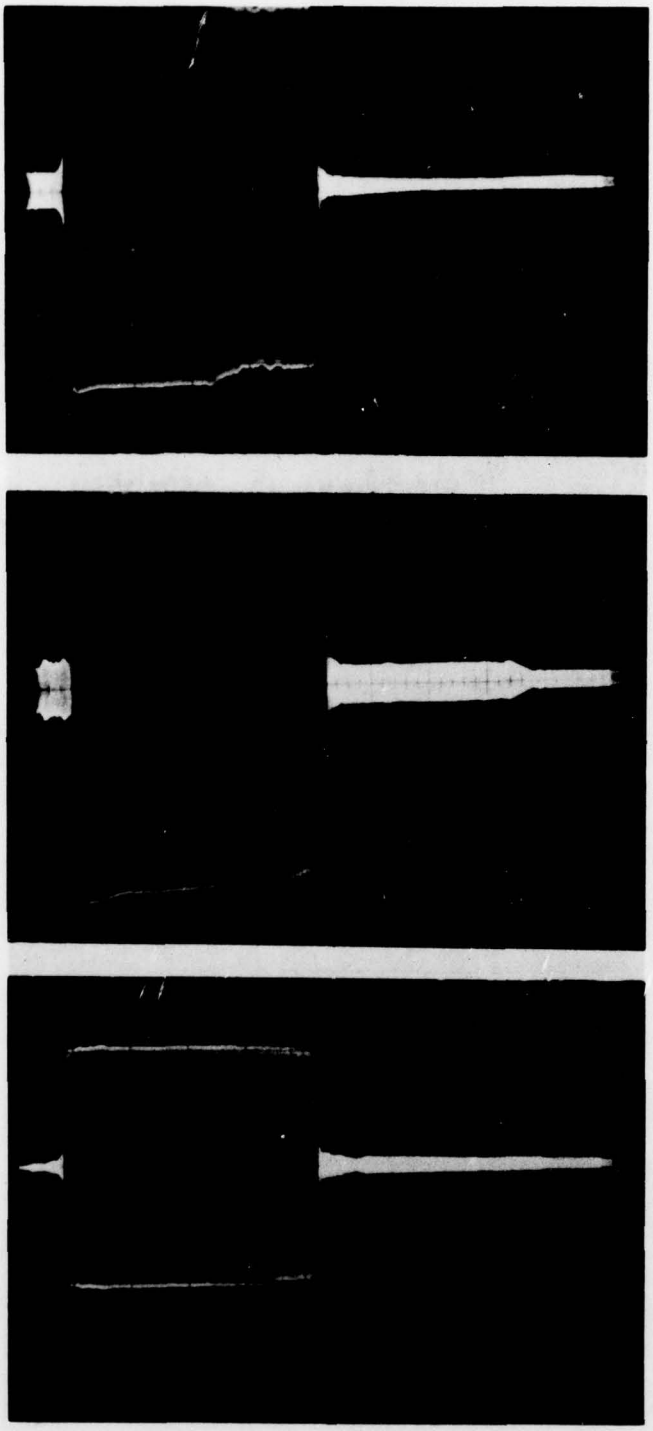

Figure 35. Delayed Signals Through the Wideband IDT's at Three Frequencies

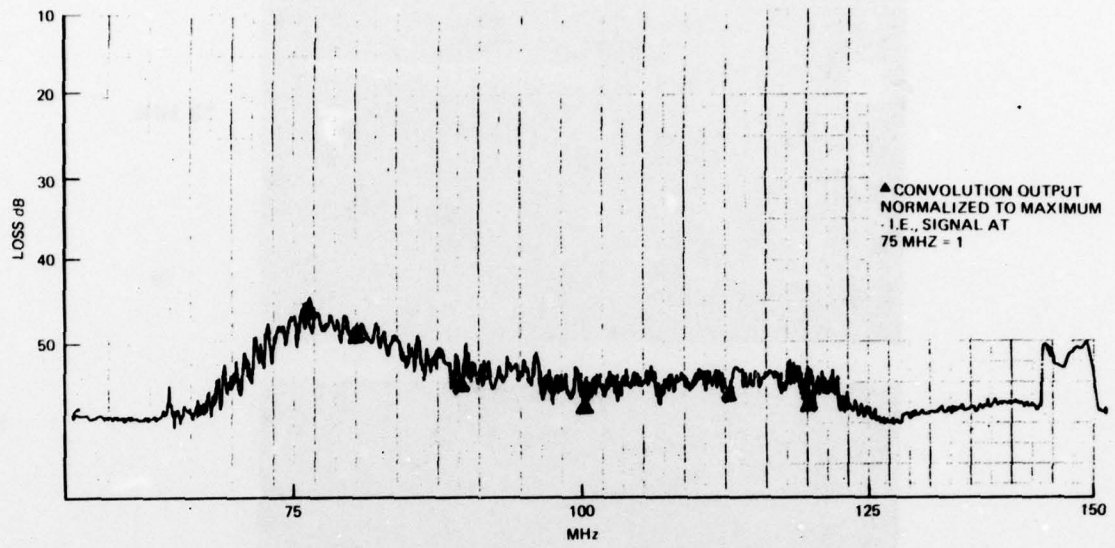

Figure 36. Convolution Output vs Frequency for Wideband IDT's

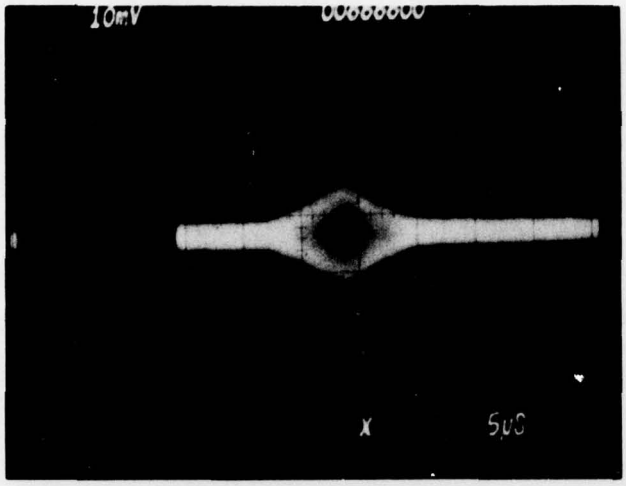

(a) DIRECT COUPLING ACROSS AIRGAP

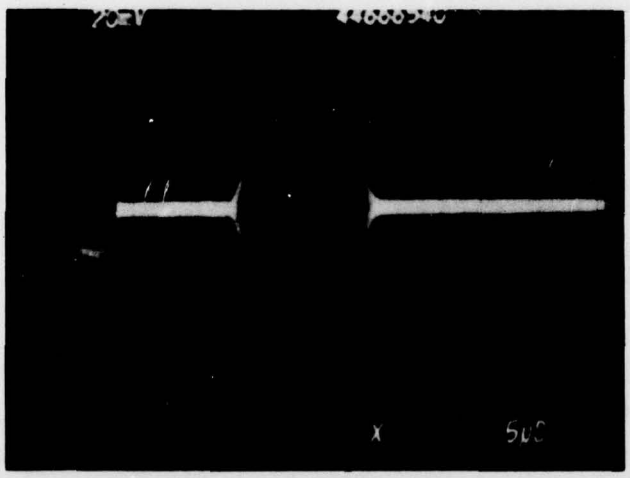

(b) STRIP COUPLED CONVOLUTION SIGNAL

Figure 37. Direct Air Gap-Coupled Output and Strip-Coupled Output

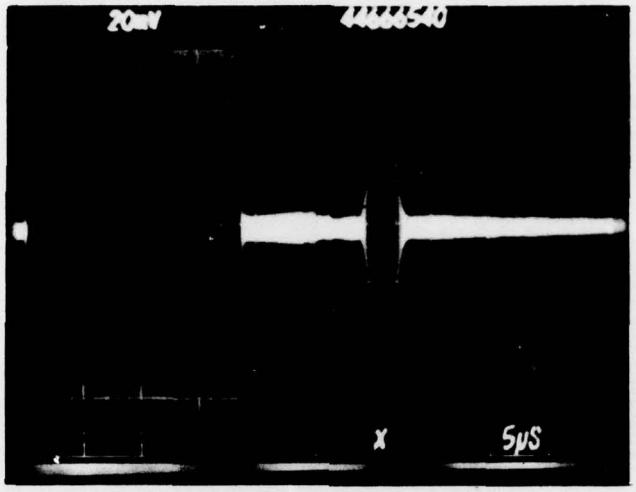

OUTPUT FROM CHANNEL 1 WITH CONTACT
ON ONLY PART OF THE INTERACTION REGION

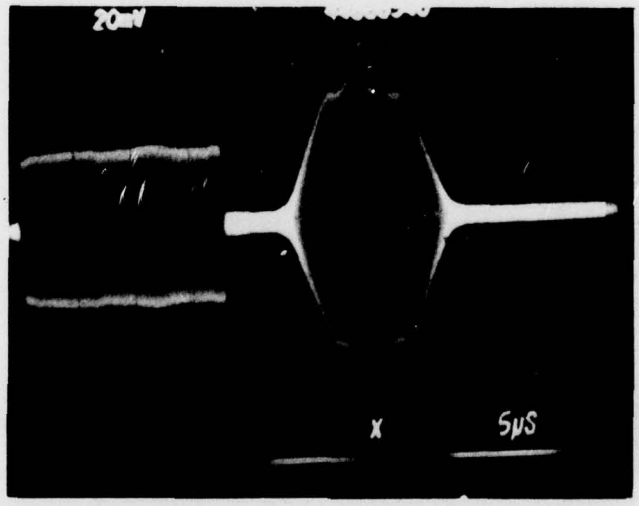

Figure 38. Single-Channel and Two-Channel Sum Illustrates the Uneven Contact Problem

TABLE 2. DEVICES TESTED

Device	Number of Channels	Interaction Time (μsec)	Bandwidth (MHz)	TB	$F_{T\ (int)}$ dBm	M(V-M/W) MEASURED	M(V-M/W) CALCULATED
1	1	11.3	7.4	83	-42	5.5×10^{-3}	4.02×10^{-2}
2	1	11.3	7.4	83	-51	1.96×10^{-3}	4.02×10^{-2}
3	2	22.6	7.4	167	-54	1.3×10^{-3}	4.02×10^{-2}
4	3	33	7.4	250	-70	2.2×10^{-4}	4.02×10^{-2}
5	1	11.3	46	519	-68	3.5×10^{-4}	4.02×10^{-2}
6	2	22.6	46	1039	-76	1.1×10^{-4}	

SECTION IV

CONCLUSIONS

The work performed during this program has demonstrated that the multichannel approach is a valid technique for achieving large time-bandwidth products with a strip-coupled convolver design. Devices with time-bandwidth products ranging from 83 to 1039 were evaluated. These time-bandwidth products are the largest ever reported for SCC's. Further devices with the best characteristics had internal efficiencies close to theoretical predictions (i.e., $F_T = -42$ dBm), and the external efficiencies of these devices were similar to those currently being obtained with $LiNbO_3$/Si air-gap convolvers ($F_T \sim -72$ dBm).

If the losses at the inputs and outputs of these devices can be reduced by 15 dB - 20 dB, convolvers with external efficiencies of up to -50 dBm (~20 dB greater than currently available) are a real possibility.

In most of the devices tested, a large fraction of the insertion loss could be reduced by reducing the resistive component of the input impedance and by designing the $R\hat{a}$ to equal 50Ω. For the best devices, the resistive component accounted for ~12 dB of the total loss. Loss from this source could be eliminated by increasing the thickness of the metallization. The problem of thin metal arises in fabricating a large number of strips of equal length over a large area, as described above. The experience gained from this work has established how much under-etching to expect and, consequently, how much wider to make the coupling strips to account for this effect. Thus, the finger resistivity problem should be greatly reduced in any future processing of SCC's. Beam steering and/or diffraction, which constitutes from 2 dB to 4 dB, can also be largely eliminated by alignment procedures in the first instance or transducer design in the second. As the coupling strips themselves contribute approximately 4 dB of insertion loss, an ultimate loss of 10 - 15 dB could be expected for a device having IDT's with optimum bandwidth and aperture. With the best devices tested during the program, this would give an external F_T of -52 to -57 dBm.

Another problem which contributes to lower efficiencies is that of maintaining a uniform contact between the silicon and the coupling strips. If for any reason there is uneveness at the silicon-strip interface -- as, for example, because of dust on the line, chip cocked at an angle, or nonuniformly applied pressure -- the signal will not fill the full interaction region and the time-bandwidth product and the efficiency will be reduced. The spring steel-ball bearing system employed for this project was not completely satisfactory and a number of modifications suggest themselves. The most satisfactory approach would be to fabricate the device monolithically with piezoelectric material and semiconductor grown on adjacent parts of the same structure, or to cement the chip in place.

To summarize, we feel that the work performed during this program has demonstrated the validity of the basic multichannel/strip-coupled concept, and that further development could produce a device with advantages over existing techniques.

SECTION V

RECOMMENDATIONS

The goal of this project was progress toward devices with time-bandwidth products up to 5,000. Using BGO, a 5000-TB device requires five channels, with substrates approximately 8 in. long. A time-bandwidth product of this magnitude was felt to be a reasonable goal, provided all losses had predicted values. Substantial progress toward the realization of the goal of large-TB devices was made. Problems were experienced with obtaining 2-μm line widths, due to the photomask's having narrower lines than gaps; this condition necessitated thinner metallization than originally planned, which, in turn, increased resistive losses in the transducers. Also the contact between the strips and the silicon was difficult to maintain with uniformity over the interaction region, further reducing efficiency. Therefore, all of the work performed on this contract was with the original design employed in somewhat easier-to-fabricate three-channel devices. These devices had potential TB's of up to 1,700 and were used to demonstrate the multichannel concept.

We feel that the results of this program are sufficiently encouraging to warrant further development of the multichannel concept for devices with large TB products. The main problems associated with the current model, namely, the fabrication difficulties and the nonuniformity of contact, were discussed in Section III. In addition to these efficiency problems, miniaturized phase shifters at the outputs will be required to ensure proper summation of the output signals for practical devices.

The use of $LiNbO_3$ will eliminate most of the processing problems experienced on this program, since $LiNbO_3$ is much harder and far more chemically inert than BGO and is readily available at substantially lower cost. The contact problem, on the other hand, is soluble by improved packaging design. Miniature phase shifters operating in the 200-500 MHz range are available, and they are suitable for the compact devices. To continue this effort, therefore, we basically recommend: (1) switching to $LiNbO_3$ as the piezoelectric substrate, (2) designing a new chip-strip contact technique, and (3) developing packaging containing all of the essential phase-shift elements. The elements of the proposed program are outlined below.

5.1 MATERIALS

In the initial stage of the continuing program, we propose using the same mask that was designed under the current contract to define structures on $LiNbO_3$. As 3-1/2-in.-long $LiNbO_3$ substrates are readily obtainable in quantity, a number of these bars could be processed simultaneously. With aluminum on $LiNbO_3$, the fabrication would be straightforward, and no major problems should be expected. Thus, with the narrowband IDT inputs, we could expect an insertion loss of no more than 15 dB and for the PRT approximately 25 dB. These figures include the approximately 5-dB loss due to the coupling strips.

Consider Eq (22) in Chapter II. For the identical geometrical parameters as used for the BGO device, an M value of 0.06 is obtained. From Eq (26), this yields a value for the internal bilinear conversion efficiency F_T of -30 dBm. Including the losses above, this would give single-channel efficiencies of -45 dBm and -55 dBm, respectively.

The device would have a time-bandwidth product of 1221. One drawback in using $LiNbO_3$ is that the higher velocity of the material dictates either a shorter interaction time nor a longer substrate. However, a given SAW structure will have a synchronous frequency on $LiNbO_3$ twice that on BGO. Therefore, if the total interaction time is less important than the time bandwidth product, one can trade off time for bandwidth and obtain the same time-bandwidth product. To increase this to 200, a new pattern which increased the length of the interaction region and raised center frequency would be designed. Taking 2 μm as a comfortable lower limit for the coupling strip width, an SCC with center frequency of 300 MHz could be readily fabricated. With the phase-reversed transducer having a bandwidth of 111 MHz, an interaction region of 6.2 cm would be required to achieve the 2000:1 TB. This could be accomplished with only three channels, as the required 2.1-cm interaction region per channel is not significantly different from that used in the current design.

5.2 SILICON/STRIP CONTACT

In order to ensure that the predicted efficiencies are achieved, the chip must be maintained in uniform contact with the coupling strips. With the spring steel/ball bearing as the arrangement used for these experiments, it was not easy to achieve repeatable results. Since all mechanical techniques have similar problems, we propose to solve this problem by permanently afixing the chip to surface.

5.3 OUTPUT PHASE SHIFTERS

To make certain that summation is achieved at the outputs, small phase shifters operating in the 200 MHz-500 MHz range will be incorporated into the package design. Analysis of the optimum input/output configurations will be performed before the design is finalized.

To see what efficiencies might be expected on $LiNbO_3$, value can be substituted into Eq (22) (Chapter II). As before, we let the stripwidth-to-coupling ratio (a/b) be equal to 0.1, and let the thickness of the oxide layer go to zero. We would expect $\Gamma/\omega c$ for $LiNbO_3$ to be similar to the BGO/Si structure, so that $\omega c/\Gamma$ would be less than one. We obtain M values of 6.5×10^{-2}, 3.25×10^{-2}, and 2.16×10^{-2} for 100 MHz, 200 MHz and 300 MHz, respectively. F_T can be calculated from Eq (26). Table 3 presents a number of possible $LiNbO_3$ devices with time-bandwidth products up to 5000 which are attainable with the multichannel SCC approach. The IDT loss column assumes no finger resistance loss. Note that the final column assumes a 2 dB/cm loss across the coupling strips and the losses associated with the dividing signal into channels.

The goal of this program continuation will be to achieve a device having a time-bandwidth product as large as practical, and which can be inserted into a system for direct comparison with existing devices. From the work performed to date, we would expect the multichannel SCC to have an efficiency of up to two orders of magnitude greater than current designs.

TABLE 3. EXPECTED EFFICIENCIES WITH LITHIUM NIOBATE

	Input Frequency	BW/MHz	Length (cm)	Channels	TB	Expected Loss (dB)	Calculated F_T (int)(dBm)	Expected F_T (tot) dBm
Preset Mask	200	14.8	5.7	3	243	12	-26.6	-38.6
	200	74.0	5.7	3	1212	25	-26.6	-51.5
	290	75.0	23.0	5	5000	16	-30.2	-46.0
	290	111.0	15.0	5	5000	30	-30.2	-60.0

REFERENCES

1. G. S. Kino and W. R. Shreve, J. Appl. Phys. 44, 3960-3968 (1973).

2. Oberdan W. Otto, paper presented at Polytechnic Institute of New York, MRI Symp. on Optical and Acoustical Microelectronics, New York (April 1974).

3. T. Aoki, M. Matuda, and S. Hattari, IEEE Trans. on Sonics and Ultrasonics, SU-25, No. 4, 213-220 (1978).